NBS TECHNICAL NOTE 1038

U.S. DEPARTMENT OF COMMERCE /National Bureau of Standards

Refracted-Ray Scanning (Refracted Near-Field Scanning) for Measuring Index Profiles of Optical Fibers

NATIONAL BUREAU OF STANDARDS

The National Bureau of Standards[1] was established by an act of Congress on March 3, 1901. The Bureau's overall goal is to strengthen and advance the Nation's science and technology and facilitate their effective application for public benefit. To this end, the Bureau conducts research and provides: (1) a basis for the Nation's physical measurement system, (2) scientific and technological services for industry and government, (3) a technical basis for equity in trade, and (4) technical services to promote public safety. The Bureau's technical work is performed by the National Measurement Laboratory, the National Engineering Laboratory, and the Institute for Computer Sciences and Technology.

THE NATIONAL MEASUREMENT LABORATORY provides the national system of physical and chemical and materials measurement; coordinates the system with measurement systems of other nations and furnishes essential services leading to accurate and uniform physical and chemical measurement throughout the Nation's scientific community, industry, and commerce; conducts materials research leading to improved methods of measurement, standards, and data on the properties of materials needed by industry, commerce, educational institutions, and Government; provides advisory and research services to other Government agencies; develops, produces, and distributes Standard Reference Materials; and provides calibration services. The Laboratory consists of the following centers:

Absolute Physical Quantities[2] — Radiation Research — Thermodynamics and Molecular Science — Analytical Chemistry — Materials Science.

THE NATIONAL ENGINEERING LABORATORY provides technology and technical services to the public and private sectors to address national needs and to solve national problems; conducts research in engineering and applied science in support of these efforts; builds and maintains competence in the necessary disciplines required to carry out this research and technical service; develops engineering data and measurement capabilities; provides engineering measurement traceability services; develops test methods and proposes engineering standards and code changes; develops and proposes new engineering practices; and develops and improves mechanisms to transfer results of its research to the ultimate user. The Laboratory consists of the following centers:

Applied Mathematics — Electronics and Electrical Engineering[2] — Mechanical Engineering and Process Technology[2] — Building Technology — Fire Research — Consumer Product Technology — Field Methods.

THE INSTITUTE FOR COMPUTER SCIENCES AND TECHNOLOGY conducts research and provides scientific and technical services to aid Federal agencies in the selection, acquisition, application, and use of computer technology to improve effectiveness and economy in Government operations in accordance with Public Law 89-306 (40 U.S.C. 759), relevant Executive Orders, and other directives; carries out this mission by managing the Federal Information Processing Standards Program, developing Federal ADP standards guidelines, and managing Federal participation in ADP voluntary standardization activities; provides scientific and technological advisory services and assistance to Federal agencies; and provides the technical foundation for computer-related policies of the Federal Government. The Institute consists of the following centers:

Programming Science and Technology — Computer Systems Engineering.

[1]Headquarters and Laboratories at Gaithersburg, MD, unless otherwise noted; mailing address Washington, DC 20234.
[2]Some divisions within the center are located at Boulder, CO 80303.

Refracted-Ray Scanning (Refracted Near-Field Scanning) for Measuring Index Profiles of Optical Fibers

M. Young

Electromagnetic Technology Division
National Engineering Laboratory
National Bureau of Standards
Boulder, Colorado 80303

U.S. DEPARTMENT OF COMMERCE, Malcolm Baldrige, Secretary

NATIONAL BUREAU OF STANDARDS, Ernest Ambler, Director

Issued May 1981

NATIONAL BUREAU OF STANDARDS TECHNICAL NOTE 1038

Nat. Bur. Stand. (U.S.), Tech. Note 1038, 56 pages (May 1981)

CODEN: NBTNAE

U.S. GOVERNMENT PRINTING OFFICE
WASHINGTON: 1981

For sale by the Superintendent of Documents, U.S. Government Printing Office, Washington, D.C. 20402

Price $3.75 (Add 25 percent additional for other than U.S. mailing)

CONTENTS

REFRACTED-RAY SCANNING (REFRACTED NEAR-FIELD SCANNING) FOR MEASURING INDEX PROFILES OF OPTICAL FIBERS

M. Young*

National Bureau of Standards
Boulder, Colorado 80303

The purpose of this work is twofold. First, it provides an elementary description and tutorial overview of the new refracted-ray method of measuring fiber-index profiles. Second, it presents new results concerning the theoretical foundation, the linearity and precision, resolution limit and edge response, and other aspects of the method. In particular, we find that index differences may be measured to 5 percent or better and spatial resolution is diffraction limited. We conclude by showing about 3 percent agreement with another laboratory and good agreement with numerical-aperture measurements performed by participants in a round-robin experiment.

Key Words: Fiber index profile; index profile; near-field scanning; optical communications; optical fiber; optical waveguide; refracted near-field scanning; refracted-ray scanning; resolution limit.

1. INTRODUCTION

Roughly a half-dozen methods have been proposed and implemented for determining the refractive-index profile of an optical-fiber waveguide. At least half of these will no doubt find use in one or another application.

One of the more promising techniques for a simple high-resolution measurement is known as refracted near-field scanning or, preferably, refracted-ray scanning. First proposed and demonstrated by Stewart [1], the method was further developed by White [2]. In addition, I have analyzed the precision of the method [3,4].

The purpose of this Technical Note is to describe refracted-ray scanning in detail, to analyze it as a measurement system, to document a particular system for implementing it, and to show some exemplary results. First, however, let us examine some of the alternate approaches that are either in use or have been proposed.

Certain methods illuminate the fiber in a direction perpendicular to the axis; that is, they look through the fiber sides rather than at its end face. These transverse-illumination methods have the advantage that they can be used to examine a fiber in real time, as it is being produced. Likewise, these methods may be used to determine the fiber's properties at several points without having to cut the fiber to prepare an end.

One of the simplest techniques is that developed by Liu, who used an oil-immersion method similar to that used in crystallography [5]. By placing a short piece of fiber in a microscope and varying the index of a matching fluid, Liu was able to measure the indices of the core and cladding of a step fiber.

*Electromagnetic Technology Division, National Engineering Laboratory

Later workers illuminated immersed fibers transversely with a laser and placed the apparatus in an interference microscope or interferometer [6-11]. The index difference between core and cladding can be obtained fairly readily and without detailed calculation [6-8], as can the alpha parameter of a fiber that is assumed to have a power-law profile [9]. In addition, formulas can be derived for calculating the full index profile from measurements of the fringe intensity [10,11]. The overall accuracy of these measurements is on the order of 10 percent, and spatial resolution is not great because the finite width of the fringes limits resolution.

Transverse-scattering methods, including backscatter, have been implemented by several groups [12-14]. With these techniques, a fiber (also immersed in oil) is illuminated transversely by a laser, and the far-field diffraction pattern is observed. A great deal of data is required, so that an automatic data-acquisition scheme is almost mandatory; the index profile is calculated by computer. The accuracy of the method is greater than of transverse interferometry, but no simple or direct methods for determining alpha or core-cladding index difference have been developed.

More recently, Marcuse and Presby have developed a focusing method that uses transverse illumination and may be used to examine either fibers or preforms [15-17]. This technique scans the near field of the transversely illuminated fiber and calculates the index profile from data acquired by a computer. Because circular symmetry is assumed in the calculation, the resulting profile is necessarily symmetric, even if the fiber is not.

Other methods illuminate the fiber along the axis; either a thin, specially prepared sample or a flat, properly prepared end is required. While not amenable to real-time measurement as a fiber is drawn nor to nondestructive testing, these methods provide a more direct evaluation of the index profile, and certain of them offer resolution that is comparable with conventional optical microscopy.

Axial or slab interference microscopy (as opposed to transverse interference microscopy) requires a thin slice of fiber to be placed in an interference microscope or interferometer [18,20]. The interferogram is generally interpreted by computer. In any case, the slab is treated purely as a phase object for the purpose of interpreting the interference pattern; because a graded-index fiber has focusing properties, it may not be regarded as a phase object unless the sample is extremely thin, say of the order of tens of micrometers. Further, it is difficult to determine what errors arise from the effects of polishing; these may include changes of the surface composition of the material and deviation from flatness as a result of the polishing rate's varying with glass composition. As with transverse interferometry, the number of fringes is small, so the spatial resolution is apt to be relatively low.

Fresnel reflection from the cleaved or polished end of a fiber has been used to measure the index profile [21,23]. This method is direct and precise and has high resolution. It is difficult because the changes in reflectance are typically less than 1 percent; highly stable radiometric techniques must be employed. This method has recently been improved with an index-matching technique [22]. However, the reflectance of the face may change as the result of contamination or exposure to the atmosphere.

Other methods that have been discussed in the literature depend on examination of the far-field interference pattern [24-26], on special properties of self-focusing fibers [27] and on the spatial coherence of the light emerging from an optical fiber [28]. (See also Ref. 29 for a more detailed review of index-profile measurements.)

2. NEAR-FIELD SCANNING

Near-field scanning depends on the existence of a local acceptance angle (or numerical aperture) at any point on the entrance face of the fiber [30]. That is, the vertex angle of the cone that can enter the fiber and be guided depends on the index of the core at the point of illumination.

The fact was first exploited by Sladen, Payne, and Adams [31,32]. This group illuminated the end of a short fiber with a uniform, lambertian source. They scanned the exit face of the fiber with a detector and thereby generated a plot of the output power as a function of position along a diameter of the fiber.

The exact proportionality between the local numerical aperture and the power coupled into the fiber holds only for guided rays. Therefore, Adams, Payne, and Sladen had to derive correction factors for the leaky-ray contribution to the power that propagates into the fiber [33,34]. With these correction factors, they are able to calculate the index profile to a high degree of accuracy.

Other workers devised a similar scheme for measuring the index profile [35,36]. Rather than illuminate the entire entrance face of the fiber, these groups focused a laser beam to a point and observed the total power radiated at the far end of the fiber as a function of the position of the point on the entrance face. This variation of near-field scanning also requires correction for leaky modes; in principle, it differs only slightly from the original technique.*

In practice, entrance-face scanning may be preferable to because an absolute calibration is possible. In addition, imperfections or mode coupling along the fiber will have minimal effect on the relative powers transmitted by excitations at different points on the entrance face. The same is not necessarily true of the exit-face scan (the original method); although I know of no detailed studies to this effect, it seems quite possible that such factors as mode coupling will distort the results in an unpredictable way, particularly in a fiber with fine structure like the characteristic index dip along the axis (see Section 8, below).

There is another difficulty with both methods of near-field scanning. This is the problem of making the leaky-mode corrections with confidence. Microbending or slight deviations of the fiber from circularity may drastically alter the leaky-mode propagation; indeed, Petermann has suggested that the leaky-mode correction may be unnecessary for fibers

*For simplicity of nomenclature and for avoiding confusion, I shall refer to both these methods as near-field scanning. When it is necessary to distinguish between them, I shall use the terms entrance-face scanning and exit-face scanning. Likewise, I will not use the term refracted near-field scanning, but rather will refer to this method as refracted-ray scanning.

with nearly square-law profiles [37]. Thus, whereas near-field scanning is both simple and elegant, it may be that its major use will be to give excellent, qualitative information about the index profile.

3. REFRACTED-RAY SCANNING

Stewart's innovation was to illuminate a fiber with a focused beam whose vertex angle greatly exceeds the acceptance angle of the fiber and to observe not the rays that are trapped by the fiber, but the rays that are refracted at the core-cladding interface [1]. With this method, it is often possible to eliminate entirely the deleterious effects of the leaky modes and to develop a system that generates the index profile directly, without the need for a correction factor.

To understand the principle of the method, it is helpful to examine Fig. 1. In that figure, a fiber whose index is n is surrounded by a liquid whose index is n_L. The fiber is illuminated by a focused cone of rays; the ray that is drawn in the figure represents the most-oblique ray in the cone, a marginal ray for the lens that focuses the beam. Because the angle of incidence exceeds the acceptance angle of the fiber, the ray is refracted both at the entrance face of the fiber and at the periphery.

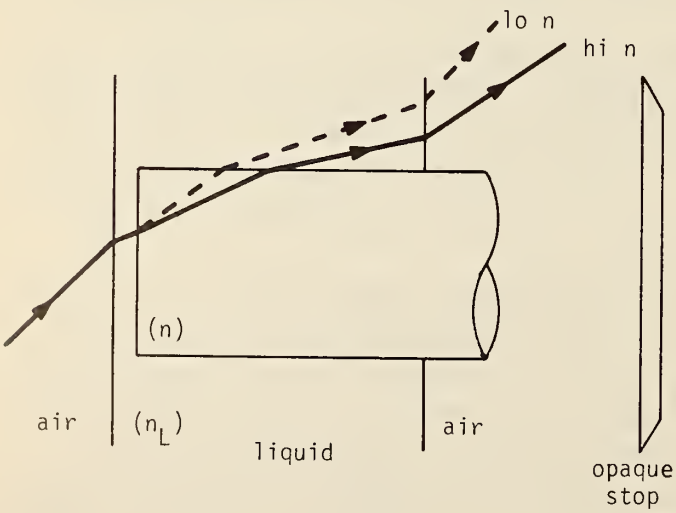

Figure 1. The lower the index of the fiber, the greater the vertex angle of the emergent cone.

Suppose now that we alter the index of the fiber in some way, for example by changing the fiber entirely. The ray that emerges is now represented by the dashed line in Fig. 1; as the index of the fiber is decreased, the angle formed by the marginal ray's intersection with the axis increases accordingly.

Now we introduce an opaque, circular stop directly behind the fiber; the stop is designed to intercept all but the outermost rays of the emergent cone. A conical shell is transmitted beyond the stop. In the plane of the stop, the inner radius of the shell is always equal to the radius of the stop. The outer radius, however, varies with the index of

the fiber. Therefore, the power that is transmitted around the stop also varies with index. The heart of refracted-ray scanning lies in the fact that, under the right conditions, the change of transmitted power is precisely proportional to the change of index of the fiber.

Figure 1 used a uniform, unclad fiber for tutorial purposes. In practice, all that is required is a fiber whose index variation is a function of radius only. The vertex of the incident cone is scanned across the entrance face of the fiber; the power transmitted by the stop is a linear function of the index of the fiber at the point of illumination.

4. STEP FIBER

For illustrative purposes, we begin by examining a meridional ray in a step fiber. The extension to the general case is straightforward.

Figure 2 traces the path of the marginal ray that is focused onto the face of the fiber. The fiber is immersed in a fluid whose index is n_L. The index of the fiber core is n; that of the cladding is n_c.

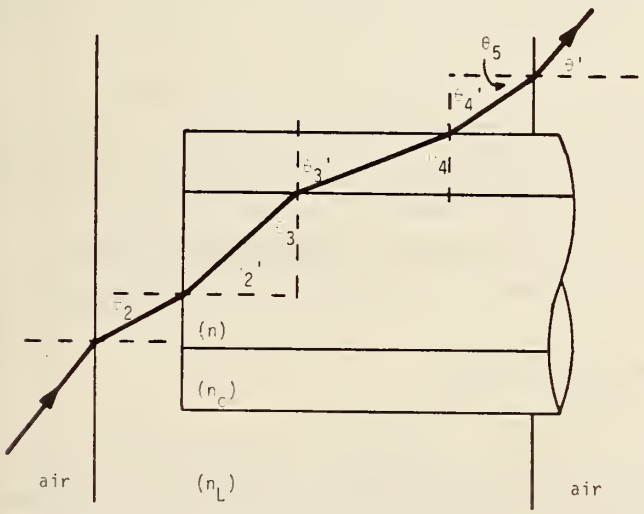

Figure 2. The path of a meridional ray through a step fiber.

The ray enters the system at angle θ to the axis of the fiber. It suffers a couple of refractions through a microscope coverslip (whose thickness is not shown) before reaching point 2. Because the coverslip makes a right angle to the axis of the system, we may easily show that

$$\sin \theta = n_L \sin \theta_2. \qquad (1)$$

$n_L \sin \theta_2$ is the numerical aperture (NA) of the cone that converges onto the face of the fiber and is equal to the NA of the microscope objective used to focus the light.

If we apply Snell's law at points 2 and 3, we find that

$$n_L \sin \theta_2 = n \sin \theta_2' , \tag{2}$$

and

$$n_c \sin \theta_3' = n \cos \theta_2' . \tag{3}$$

If we square and add these equations and use Eq. (1), we find that

$$\sin^2 \theta + n_c^2 \sin^2 \theta_3' = n^2 . \tag{4}$$

We may eliminate the term in θ_3' by applying Snell's law at points 4 and 5:

$$n_c \sin \theta_3' = n_L \sin \theta_4' , \tag{5}$$

and

$$\sin \theta' = n_L \cos \theta_4' . \tag{6}$$

Finally, we square and add Eqs. (5) and (6) and combine with Eq. (4) to learn that

$$n^2 = n_L^2 + \sin^2 \theta - \sin^2 \theta'. \tag{7}$$

Equation (7) shows how the vertex angle θ' of the emergent conical shell of rays is related to the core index n of the fiber.

5. A MORE-GENERAL CASE

Consider the general case of a skew ray incident on a graded-index fiber with angle of incidence θ and arbitrary azimuthal angle ϕ; this is shown in Fig. 3, with the cover slip omitted for clarity.

Snell's law may be written as

$$n \sin i = \text{constant}, \tag{8}$$

where i is the angle of incidence at an arbitrary interface. Equation (8) is valid whether the index change is sudden or gradual. If λ is the vacuum wavelength of light, then the magnitude k of the wavevector in a medium is $2\pi n/\lambda$; therefore, Snell's law may also be written in the equivalent form,

$$k \sin i = k_\perp = \text{constant}. \tag{8a}$$

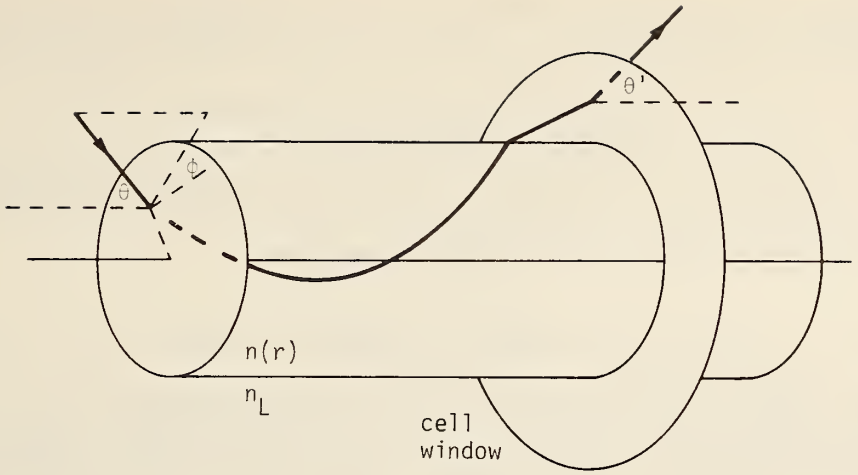

Figure 3. The path of a skew ray through a graded-index fiber. θ is the angle of incidence, and ϕ, which lies in a plane perpendicular to the axis, is the azimuthal angle. The coverslip at the front of the cell is suppressed for clarity.

That is, the component of the wave vector perpendicular to the index gradient is conserved as the ray propagates. White has used this principle to derive a general form of Eq. (7). It is applicable to any fiber whose index variations are purely radial.

Let us number points 1 through 5 as in Fig. 2, remembering, however, that the ray path inside the fiber is in general curved and need not lie in a plane. Using Eq. (8a), we find that

$$\sin \theta = n_L \sin \theta_2 = n(r) \sin \theta_2' \ . \tag{9}$$

where n(r) is the index of the fiber at a distance r from the axis of symmetry. From point 2 until point 4, the index variations become purely radial, so the axial component of the wave vector remains constant; that is,

$$n(r) \cos \theta_2' = n_L \cos \theta_5 \ . \tag{10}$$

Finally, at point 5,

$$n_L \sin \theta_5 = \sin \theta' \ . \tag{11}$$

Combining Eqs. (9) through (11) as before, we find that

$$n^2(r) = n_L^2 + \sin^2 \theta - \sin^2 \theta'. \tag{12}$$

This is the same as Eq. (2) of Ref. 2. When $n(r)$ is nearly equal to n_L we may rewrite Eq. (12) in the form

$$2n_L \Delta n(r) = \sin^2 \theta - \sin^2 \theta'. \tag{12a}$$

$\Delta n(r) = n(r) - n_L \ll n(r), n_L$; it is not the delta parameter of the fiber. We discuss the importance of Eqs. (12) and (12a) in the following sections.

6. RADIOMETRIC ANALYSIS

A lambertian source is one whose radiance is independent of angle. Many thermal sources approximate lambertian sources; lasers and many light-emitting diodes do not. We begin this section by assuming that the source is lambertian and later generalize to a non-lambertian case.

Into a cone whose vertex angle is θ', a lambertian source emits total power proportional to $\sin^2 \theta'$ [38]. In the refracted-ray technique, we insert an opaque stop behind the fiber to block some of the rays refracted by the fiber, as in Fig. 1. If the source is lambertian, then the power transmitted around the stop may be expressed as

$$P(\theta') = A (\sin^2 \theta' - \sin^2 \theta_s), \tag{13}$$

where θ_s is the angle subtended by the stop and A is a constant of proportionality.

If we let $n(r) = n_L$ (no fiber in the system), then we find from Eq. (12) that $\theta' = \theta$. If we call the power transmitted around the stop P_o, then we find that

$$A = P_o/(\sin^2 \theta - \sin^2 \theta_s). \tag{14}$$

Finally, if we combine Eqs. (12a), (13) and (14), we find that

$$2 n_L \Delta n(r) = \frac{P(\theta') - P_o}{P_o} (\sin^2 \theta - \sin^2 \theta_s). \tag{15}$$

All the terms in this equation are constants except $P(\theta')$ and $\Delta n(r)$. Thus, when Δn is small, the power that propagates beyond the stop is in principle precisely proportional to the index profile of the fiber. (The derivation has been made for guided rays only; see Ref. 2 and below for a discussion of leaky rays.)

Equation (15) could be used for calibration of the system if the two angles, θ and θ_s, could be measured with sufficient precision. In particular, it is difficult to measure θ_s, because this is the angle subtended by the stop at a point inside the fiber--that is, at the virtual image of the point source as seen from the rear of the cell. In part for this reason, it may be preferable to devise a direct calibration method (see Section 11, below).

Many sources are not lambertian. For example, a laser beam that is expanded and passed through a small-diameter lens more nearly approximates a uniform point source than a lambertian source. In contrast, edge-emitting diodes and semiconductor lasers emit their radiation more strongly in the forward direction than does a lambertian source. Such sources can be approximated at least roughly by writing their radiance $L(\theta)$ in the form,

$$L(\theta) = L_o \cos^m \theta \ , \tag{16}$$

where we assume circular symmetry. A lambertian source is described by m = 0 and a uniform point by m = -1. Other sources, such as edge-emitting diodes, may be approximated by using Eq. (16) with m an integer between, say, 5 or 10, depending on the specific source.

As noted above, the power radiated by a lambert source into a cone is proportional to $\sin^2\theta$; see, for example, Eq. (3.17) of Ref. 35. If we follow the derivation leading to that equation, we find that the fraction of the total power radiated into a cone is

$$1 - \cos^{m+2} \theta, \tag{17}$$

which reduces to $\sin^2 \theta$ when m = 0. (This relationship and all subsequent ones are also valid when m = -1.) Equation (13) becomes, in the general case,

$$P(\theta') = A \ (\cos^{m+2} \theta_s - \cos^{m+2} \theta') \ , \tag{18}$$

and Eq. (14) becomes

$$A = P_o/(\cos^{m+2} \theta_s - \cos^{m+2} \theta) \ . \tag{19}$$

If Eq. (18) is to describe the fiber index profile, it must be linear in $\sin^2 \theta'$, because Eq. (12a) shows that $\Delta n(r)$ is linear with $\sin^2 \theta'$. I have not found it fruitful to try to relate Eq. (18) directly with $\sin^2 \theta$; however, it is instructive to plot $(1 - \cos^{m+2} \theta)$ [Eq. (17)] as a function of $\sin^2 \theta$. This is shown in Fig. 4 for several values of m.

The most-important cases are the lambertian source and the uniform point source, for which m is equal to 0 and -1. The former case is obviously linear, and the latter is nearly so for numerical apertures up to 0.6 or more. Fortunately, what is important is that the curves be linear only over the small range of angles defined by the stop diameter and the numerical aperture of the focusing lens.

As m increases, the curves become less linear. Also, they deviate substantially from the line m = 0. Therefore, unless m is precisely 0, a calibration based on Eq. (15) will be invalid.

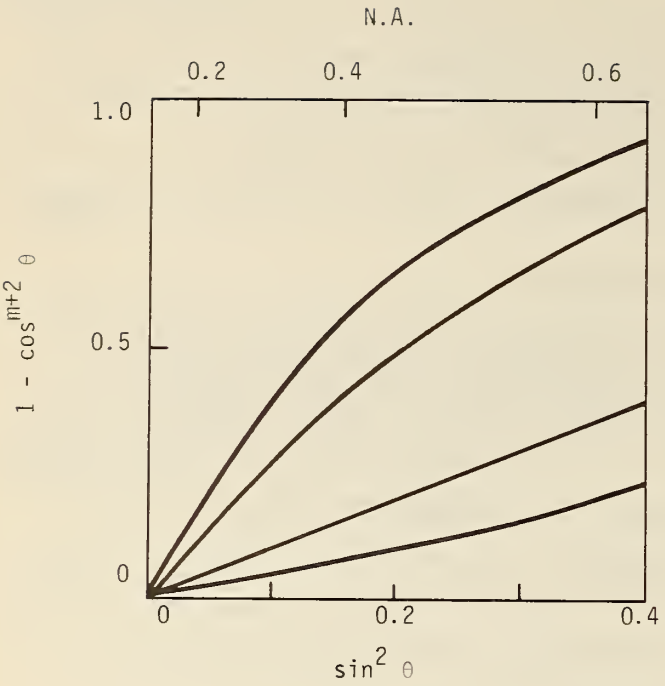

Figure 4. A function useful for describing the power transmitted by a non-lambertian source.

7. LEAKY-RAY ANALYSIS

Suppose that a circular fiber is illuminated off axis by a focused cone of rays. Geometric optics predicts that certain rays will be trapped by the fiber, whereas certain others will be refracted out of the fiber; we refer to these cases as guided and refracted rays (or bound and radiation modes).

Snyder and his colleagues have shown that certain rays are not truly guided but nevertheless suffer high loss and therefore are greatly attenuated after transmission along a relatively short length of fiber; they called these leaky rays [39-41]. The presence of leaky rays invalidates a guided-ray analysis such as that of Sections 4, 5 and 6.

Adams, Payne and Sladen have derived correction factors to be used with the near-field scanning technique [33,34]. However, as noted above, there is some doubt as to the utility of these correction factors in some cases. The refracted-ray technique in many cases avoids the necessity for a correction factor by adjusting the angular subtense of the stop so that the leaky-ray power transmitted by the fiber is intercepted by the stop; only truly refracted rays are passed by the stop. When the leaky-ray contribution is excluded, the guided-ray analysis becomes valid [33].

If a fiber is excited at a point at a distance r from the center, leaky rays will be excited only for angles of incidence θ given by [2,41]

$$(n^2(r) - n_c^2) / (1 - \rho^2 \cos^2 \phi) \geq \sin^2 \theta > n^2(r) - n_c^2. \qquad (20)$$

ϕ is the azimuthal angle shown in Fig. 3, a is the core radius and ρ is (r/a); all other terms have been defined before.

Following White, we exclude leaky rays by restricting angles of incidence to values larger than the largest value of the left side of Eq. (20). That is, we make the opaque stop large enough that rays pass the stop only if their angle of incidence is larger than that given by

$$\sin^2 \theta > (n^2(r) - n_c^2)/(1 - \rho^2). \tag{21}$$

The right side of this equation defines the largest angle of incidence at which leaky rays will be excited at a given radius.

If we apply Eq. (11) to Eq. (21), we find that leaky rays will be excluded provided that θ_s exceeds the value of θ' given by

$$\sin^2 \theta_s > \sin^2 \theta' = n_L^2 - n^2(r) + [(n^2(r) - n_c^2)/(1 - \rho^2)] . \tag{22}$$

White has applied Eq. (22) to a fiber with a power-law profile and quoted his results [2]. A power-law profile may be described by the equations

$$n^2(r) = n_o^2 (1 - 2\rho^\alpha \Delta) , \tag{23a}$$

and

$$n_c^2 = n^2(a) = n_o^2 (1 - 2\Delta) , \tag{23b}$$

where

$$n_o = n(0) \text{ and } \Delta = (n_o^2 - n_c^2)/2n_o^2. \tag{23c}$$

If we use these equations in Eq. (22), we find after a few lines of algebra that

$$\sin^2 \theta_s > (n_L^2 - n_c^2) + 2n_o^2 \rho^2 \Delta (1 - \rho^\alpha)/(1 - \rho^2), \tag{24}$$

which is the same as White's Eq. (10) [2].

To eliminate the leaky rays entirely, we must examine Eq. (24) when the ρ term on the right side is largest. Physically, it is clear that this term must be a maximum when $\rho = 1$, because leaky rays are excited in greater numbers as we move away from the axis toward the core-cladding interface. We may also show this analytically by letting $R = \rho^2$ and differentiating F(R), where

$$F(R) = R(1 - R^x)/(1 - R) \tag{25}$$

and $x = \alpha/2$. The derivative is equal to

$$dF/dR = [1 - (1+x)\ R^x + x\ R^{x+1}](1 - R)^{-2}, \tag{26}$$

which is indeterminate when R = 1. We may evaluate the limit by substituting R = 1 - ε and letting ε → 0. We find in this way that the derivative is indeed 0 when R = 1, and that F(R) is a maximum at the core-cladding boundary.

Returning now to Eq. (24), we evaluate F(R) in the limit R → 1 by applying l'Hôpital's rule. The calculation is straightforward and leads to the conclusion that F(R) approaches α/2 as R approaches 1.

Thus, the angular subtense of the stop must exceed

$$\sin^2 \theta_s > (n_L^2 - n_c^2) + n_o^2\ \alpha\ \Delta\ , \tag{27}$$

which is equivalent to Eq. (13) of Ref. 2.

If the parameters in Eq. (27) are reasonably well known, then it is an easy matter to calculate the minimum stop diameter. In the event that all the parameters are not known, then it is possible to measure the first term on the right side of Eq. (27). Let I be the axial acceptance angle of the fiber. Then, according to Ref. 2 or Ref. 38, Section 2.8,

$$\sin^2 I = n_o^2 - n_c^2\ . \tag{28}$$

We now return to Eq. (11) and replace θ and θ' with I and I', where I' is the angle at which the guided ray emerges from the cell. Combining Eqs. (11) and (27) in this way shows that

$$\sin^2 I' = n_L^2 - n_c^2\ . \tag{29}$$

Thus, the term $(n_L^2 - n_c^2)$ in Eq. (27) is equal to $\sin^2 I'$, where I' is the inner vertex angle of the hollow cone of light that is refracted by the fiber. An alternate way of writing Eq. (27) is therefore to replace $(n_L^2 - n_c^2)$ with sin I'.

Finally, $2n_o^2\Delta$ is equal to $\sin^2 I$, where sin I is sometimes called the theoretical numerical aperture of the fiber. Therefore, Eq. (27) may be rewritten

$$\sin^2 \theta_s > \sin^2 I' + (\alpha/2) \sin^2 I. \tag{30}$$

The stop must subtend an angle larger than the value of θ' given by Eq. (27) or (30). By way of example, let us choose a fiber for which $n_c = 1.46$ (approximately the value for vitreous silica), sin I = 0.25, and α = 2.3. Assume further that n_L is one-half percent larger than n_c (it is preferable to choose $n_L > n_c$ to avoid exciting cladding modes). I have chosen these values deliberately to overestimate sin θ.

Using Eqs. (29) and (30), we find that $\sin^2 I' = 0.021$ and therefore that $\sin \theta_s > 0.3$. A microscope objective with a numerical aperture in the neighborhood of 0.5 will be required; fortunately these are quite common.

A profile with an index step may be thought of as a power-law profile for which α approaches infinity. According to Eq. (30), there is no value of θ_s for which leaky rays can be completely excluded if α is unbounded.

When $r = 0$, θ' is a minimum (we exclude from this discussion the possibility of an index dip at the center). Therefore, to allow observation of the complete index profile, the angular subtense of the opaque stop must not exceed the value of θ' given from Eq. (11) by

$$\sin^2 \theta_s < \sin^2 \theta' = \sin^2 \theta + n_L^2 - n_0^2, \tag{31}$$

which is just Eq. (11) with $r = 0$. We may write n_0 in terms of Δ by manipulating Eq. (23c), which yields

$$n_0^2 = n_c^2 + N_F^2, \tag{32}$$

where $N_F = \sin I = 2n_0^2\Delta$. The second equality holds because Δ is very small. Using Eq. (32) in Eq. (31), we find that

$$\sin^2 \theta_s < \sin^2 \theta + n_L^2 - n_c^2 - N_F^2 , \tag{33}$$

which is White's Eq. (15) [2].

Equation (31) or (33) delimits the angular subtense of the largest stop that may be used with a given fiber. Equation (24) delimits the greatest angle of refraction at which leaky modes will be found. This angle increases with radius. Following White, let us assume that the subtense of the stop is precisely that given by Eq. (33); in fact, it must be slightly less than this value. If we scan a fiber, leaky modes will not appear beyond the stop until the radius is sufficiently large that the angle θ' defined by Eq. (24) exceeds the subtense of the stop as given in Eq. (33). To find an implicit expression for this radius, we set the right sides of these two equations equal and find that

$$N^2/N_F^2 = (1 - \rho^{(\alpha+2)})/(1 - \rho^2) \tag{34}$$

where $\rho = (r/a)$, and $N = \sin \theta$ is the numerical aperture of the incident cone.

We calculate the limit of Eq. (34) as ρ approaches 1 and solve for α. Because $\rho = 1$ at the core-cladding interface, this procedure yields the largest value of α for which leaky modes will not be a factor. The calculation is carried out using l'Hôpital's rule; the result is

$$\alpha = 2[(N^2/N_F^2) - 1] , \tag{35}$$

which is Eq. (18) of Ref. 2. For a fiber for which sin I is 0.25 illuminated by a microscope objective whose NA is 0.5, $\alpha = 6$; α increases to 10.5 if sin I decreases to 0.2. Thus, leaky rays can be handled for nearly all practical fibers except possibly step fibers.

For step fibers, we examine Eq. (34) in the limit as $\alpha \to \infty$. Because ρ is at most 1, the right side simply approaches $1/(1 - \rho^2)$. Therefore,

$$r/a < (1 - N_F^2/N^2)^{1/2} \tag{36}$$

for leaky rays to be excluded by the stop. This relation is precise only when θ_s has been optimized for each fiber. For the examples used in connection with Eq. (35), $\rho = 0.87$ and 0.92, in that order. Beyond these radii, an indeterminate fraction of the leaky-ray power is blocked by the stop; therefore, it is not possible to calculate a correction factor. Thus, the refracted-ray method is not useful for scanning step fibers beyond about nine tenths of their radius.

8. RESOLUTION LIMIT, EDGE RESPONSE AND DEPTH OF FOCUS

White has argued that the spatial resolution limit of the system is limited by the opaque central stop [2]. The stop lies roughly in the entrance pupil of the condensing lens, and it is natural to project the stop into the exit pupil of the microscope objective, where it obscures the appropriate fraction of the exit-pupil diameter. Because the microscope is diffraction limited, the resolution limit may be expected to be that of a diffraction-limited annular aperture.

This argument would be precisely correct if the condensing lens were itself a diffraction-limited imaging lens; in that case, the resolution limit in the image plane of the condensing lens would be determined by the annular stop, which could be projected to any convenient point of the optical system.

Born and Wolf have calculated the Fraunhofer-diffraction pattern of a circular aperture, a fraction ε of whose diameter is obscured by an opaque circular stop [42]; it is

$$I(\beta) = [2J_1(\beta)/\beta - 2\varepsilon^2 J_1(\varepsilon\beta)/(\varepsilon\beta)]^2/(1-\varepsilon^2)^2 , \tag{37}$$

where J_1 is the Bessel function of order 1, $\beta = (\pi/\lambda)\, D \sin\theta$ is the normalized dimension in the image plane, D is the exit-pupil diameter, θ is the angle by which the observation is off axis, and the intensity at the center of the pattern is 1. The radius of the Airy disk (first zero of the Bessel function) of a clear aperture occurs where $\beta = 1.22\pi$.

Equation (37) describes the impulse response or point-spread function of a lens with an annular aperture. When we scan a fiber, we translate the point-spread function at right angles to the index variations of interest. Therefore, we require knowledge of the edge response of the lens, rather than the impulse response [43]. This is the convolution of the impulse response with a unit step in the direction normal to the direction of translation;

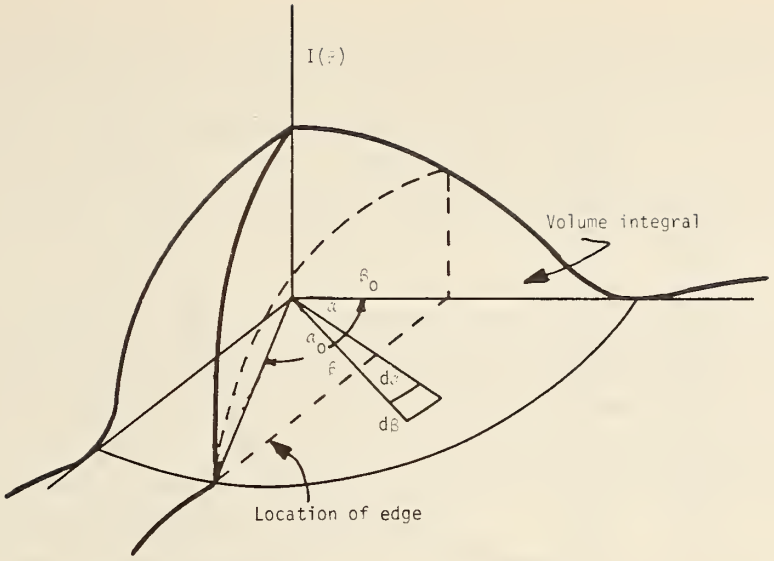

Figure 5. Geometry used to calculate the edge response of a diffraction-limited lens with a central stop.

it may be calculated by carrying out the volume integral indicated in Fig. 5, in which the sombrero-like function represents Eq. (37). The integration,

$$2 \int_0^{\alpha_0} \int_0^{\infty} I(\beta)\ \beta\ d\beta\ d\alpha \qquad (38)$$

has been carried out numerically for values of ε between 0 and 0.9 [44]. is the angle shown in Fig. 5. Although the edge response is defined for an opaque edge, it should approximately describe the response of an optical system to the sharp index step of interest to us.

We may define the edge-response width in a manner analogous to the definition of rise time or transition duration in electrical engineering: The edge-response width is the distance between the two points where the intensity of the image is 10 percent and 90 percent of the maximum. This parameter gives a measure of the resolution limit of the system as a function of the normalized stop diameter ε.

The solid curve of Fig. 6 shows the edge-response width as a function of relative stop diameter ε. The ordinate is normalized to the Airy-disk radius, so the graph has universal applicability. When $\varepsilon = 0$, the edge-response width is very close to the Rayleigh limit; this is in good agreement with measurements of resolution of bar targets. (Incidentally, the curve lies very close to the function $1/(1-\varepsilon)$, which is what I guessed by replacing D with $D(1-\varepsilon)$ in the expression for the Airy-disk radius.)

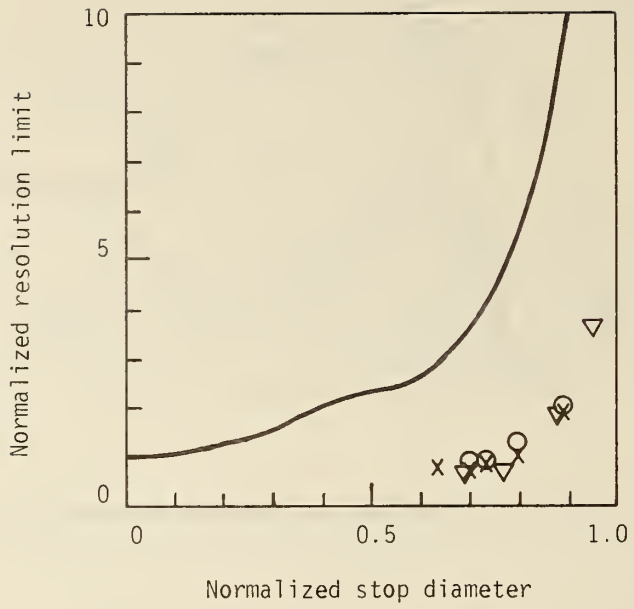

Figure 6. Resolution limit as a function of central stop diamter for the case of a diffraction-limited lens. Solid line is the calculated edge response: experimental points are measured index-step widths.

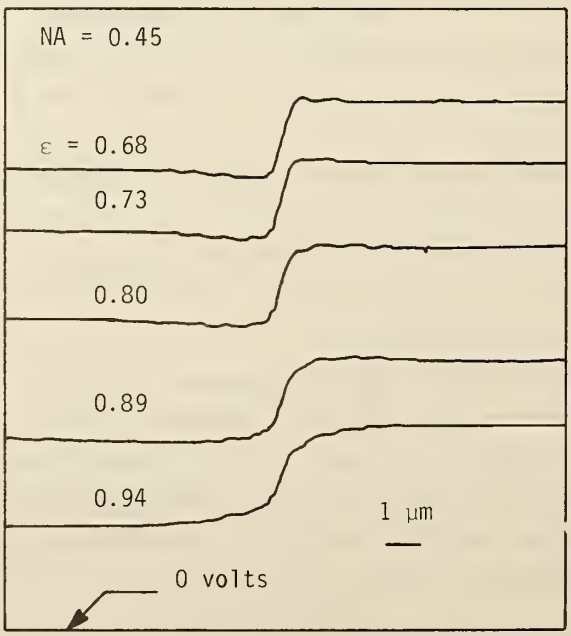

Figure 7. Measured edge response of refracted-ray scan for various values of ε.

To measure the edge-response width of the refracted-ray scanning system (to be described shortly), I cleaved some home-made quartz fibers, immersed them in oil, and scanned across the edge along a diameter that was roughly at right angles to the direction along which the fiber had been cleaved. Figure 7 shows a typical set of such scans for several values of ε. This parameter varies by about 10 percent depending upon whether the light is focused into the fiber or the oil; the numbers in Fig. 7 are the averages of these two values.

Data derived from the scans of Fig. 7 and other scans are shown as discrete points in Fig. 6. Whereas there is slight effect from increasing ε, the data do not agree well with the theory and show that resolution is diffraction limited as long as ε is less than 0.8. (These data at least roughly agree with White's; however, White's approximate calculation does not agree with the curve of Fig. 3, which was generated without recourse to a gaussian approximation to the sombrero function, $2J_1(x)/x$.)

The condensing lens is merely a collector of light and does not project a high-quality image. Indeed, it may be thought of as a part of the detector, for the system would be unchanged if the condensing lens and detector were replaced by a single, large detector. Thus, we may regard the refracted-ray apparatus as a scanning microscope that uses an annular detector.

Kermisch has pointed out that a scanning microscope is precisely equivalent to a conventional imaging system, provided that the detector be replaced with an incoherent source, and the source with a point detector [45]. Therefore our system is equivalent to a microscope with a central stop in the condenser optics; its resolution limit (and other characteristics) may be analyzed by performing calculations on this equivalent system. Considerations based on the Abbe theory show that the resolution limit ought to be roughly constant as the size of the central stop is increased. (An extreme case is dark-field microscopy; similar considerations show that resolution is comparable to that of conventional, bright-field microscopy and can even be slightly better [46].) At any rate, the resolution limit of conventional microscopy changes by no more than 30 percent or so as varying conditions of illumination result in different degrees of coherence [42].

Change of the stop's angular subtense is equivalent to a similar change of illumination in conventional microscopy. Therefore, we expect the resolution limit of our system to vary only slightly with changing stop position, and this indeed seems to be the case. I cannot at present account for the sudden loss of resolution at large values of ε.*

Depth of focus is related to resolution limit and is one factor that may determine the precision with which the end of the fiber must be perpendicular to the axis of the system. For a diffraction-limited optical system such as a microscope objective, depth of focus may be written [47]

$$DF = n\lambda/2(NA)^2. \tag{39}$$

* Footnote added in proof: W. J. Stewart has shown that the resolution limit is actually a minimum for certain values of ε; that is, resolution limit increases as ε is decreased below the values examined in this paper. Using these results, Reid and Stewart have succeeded in developing a system with 0.35 μm resolution limit [48,49].

If NA = 0.5 and λ = 633 nm, the depth of focus DF is about 2 μm. If we focus on the center of a 100-μm diameter fiber, then the edges will be in sharp focus only if the face of the fiber deviates from perpendicularity by less than (2/50) rad, or about 2°.

9. CONDENSING LENS

With no fiber in the cell, the hollow cone transmitted through the cell will have a numerical aperture NA equal to that of the microscope objective. If the fiber index is slightly less than that of the matching fluid, then the cone angle is increased slightly but is still of the order of the incident cone angle. The hollow cone must be focused by a condensing lens onto a detector.

Lenses (other than microscope objectives) are more commonly described in terms of their F number ϕ than numerical aperture. Figure 8 shows the geometry used for calculating the relationship between NA and F number. In air, the NA is given by

$$NA = \sin U = D/2(f'^2 + D^2/4)^{1/2} \tag{40}$$

from which we may readily calculate that

$$\phi = f'/D = (1/2)(NA^{-2} - 1)^{1/2} \tag{41}$$

Thus, an NA of 0.5 is equivalent to an F number of about 0.9. (Table 1 compares NA and F number.) We must design a condensing lens with an effective F number ϕ(1 + magnification) less than 1 [50].

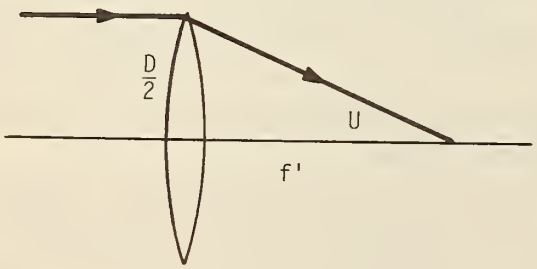

Figure 8. Vertex angle of a lens.

Table 1

F Number, Numerical Aperture, and Vertex Angle

NA	ϕ	U
0.15	3.3	8.6°
0.20	2.4	12
0.25	1.9	15
0.40	1.15	23.5
0.50	0.87	30
0.65	0.58	41

Single-element condensing lenses may be purchased readily with F numbers of 2 or somewhat less. To achieve an effective F number less than 1, we must design a compound lens, the first element of which is operated with the object distance about one half the focal length.

To minimize the aberrations of the lens, we attempt to make the deviation of the ray by each lens a constant; likewise, we choose the elements in such a way that the deviation at each surface is about one half the total deviation of the lens.

Figure 9 shows a thin lens whose focal length is f' projecting an image with conjugates ℓ and ℓ'. The angles u and u' are defined as shown, as is the deviation δ. The theorem concerning the external angle of a triangle shows that

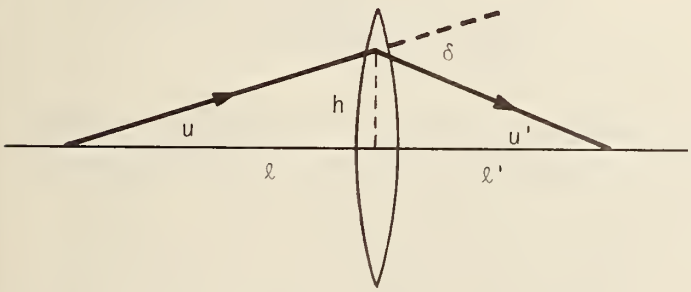

Figure 9. Deviation and other parameters of the condensing lens.

$$\delta = u + u'. \tag{42}$$

This result is true for thick lenses as well as thin. In paraxial approximation,

$$u = h/\ell , \tag{43a}$$

and

$$u' = h/\ell'. \tag{43b}$$

Using Eq. (42) and the lens equation, we find immediately that

$$\delta = h/f'. \tag{44}$$

Now consider a three-element condensing lens (Fig. 10). For the moment, consider the lenses to be thin and in contact; all have focal length f'. If we demand a magnification m = 2, then the image distance ℓ_3' is equal to $2\ell_1$, where ℓ_1 is the object distance. If the deviation by each lens is δ, then the total deviation is 3δ; therefore, looking at the lens as a whole, we find that

$$3\delta = (h/\ell_1) + (h/2\ell_1). \tag{45}$$

Because $\delta = h/f'$ the object distance ℓ_1 is $f'/2$.

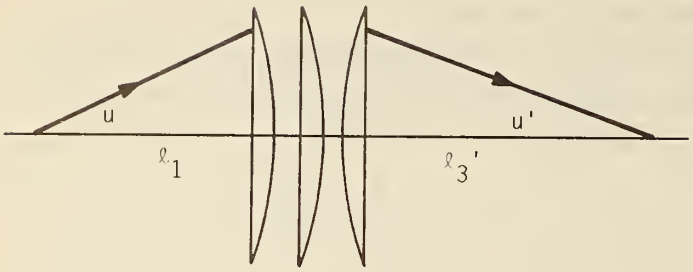

Figure 10. Conjugates of the three element condensing lens.

A simple, paraxial ray trace using the lens equation shows that the first lens projects a virtual object to the primary focal point of the second lens; the second lens projects the image to ∞; and the third lens projects the image to its secondary focal point. Thus, to minimize spherical aberration, the lenses should be planoconvex, each oriented with its curved side toward its own long conjugate. (The first element should in principle be meniscus, but such a lens may not be available.) If the lenses have been molded and are to be placed into a barrel, they must be centered and have their edges ground by an optics shop to keep other aberrations to a minimum. Image quality is still poor, as with all condensing lenses, so a uniform, large-area detector is required.

In reality, the elements are comparatively thick with respect to their focal lengths. Therefore, it may be necessary to follow the path of a marginal ray through the lens to be certain that one of the central elements does not act as the aperture stop for the system. Apart from this caveat, the design based on thin-lens elements is probably adequate. The effective focal length of the real lens will exceed the calculated value somewhat.

For most cases, a three-element lens working at the magnification of 2 will probably be adequate; if not, a four-element lens may be necessary. It is easy to generalize Eq. (44) to the case of an N-element lens with magnification m. The result of an analysis exactly similar to the preceding is

$$\ell_1 = (1 + 1/m)\ f'/N\ , \tag{46}$$

$$\ell_N' = (1 + m)\ f'/N\ , \tag{47}$$

where ℓ_N' is the image distance.

Finally, the design of the condenser is complicated and could lead either to a very large lens or to a thick lens with barely sufficient clearance between the lens and the end of the capillary. W. C. Meixner of Valtec suggested the use of plastic Fresnel lenses

instead. Aspheric Fresnel lenses are available from more than one manufacturer with F numbers as low as 0.7. These lenses are corrected for spherical aberration, generally provided that one conjugate is at infinity. Therefore, two lenses with equal diameter (but not necessarily equal focal length) will be required: The first roughly collimates the beam, and the second focuses onto the detector. The F number of 0.7 implies that the numerical aperture of the microscope objective may exceed 0.5 if necessary. Much of the experimental work, including the final calibration run and fiber scans, reported in the remainder of this paper was carried out after a Fresnel-lens condenser had been installed.

10. APPARATUS

The experimental apparatus is sketched in Fig. 11. The HeNe-laser beam is expanded by the first microscope objective MO and focused by the second 40X microscope objective through a microscope cover slip onto the fiber. The fiber is held in the moveable cell, whose cross section is shown in Fig. 12 and which is discussed below. The fiber passes through a hole in the opaque stop OS. The refracted rays escape the fiber and are focused by the condensing lens CL onto a uniform, 1-cm-diameter silicon detector. The lens is designed as described in the previous section; the elements have 127-mm focal length and 9-cm diameter and are fixed in an aluminum housing as shown in Fig. 13. Because the laser is polarized, the $\lambda/4$ plate is used to reduce the dependence of various reflectances on angle.

Figure 14 shows two rear views of the apparatus, with the lens and detector removed. The cell is constructed of aluminum. The glass window is fastened with a good grade of epoxy. The cover slip is fastened to a mounting plate with a fast-setting epoxy that may be removed with a razor blade if the cover slip has to be replaced; the plate is screwed to the cell housing in case the cover slip must be removed and cleaned. The fiber is introduced through a 0.25-mm capillary tube that is fastened to the window with the same rapidly setting epoxy, so that the capillary tube may be removed easily with a heat gun. The outer end of the tube has been formed into a funnel to guide the fiber. The stop is made of aluminum by turning it on a lathe and is fixed in place with piano wire, as shown in Fig. 15. Stray light that passes through the hole in the stop is intercepted by a piece of black tape fastened to the center of the lens.

In addition, I illuminate the fiber with a white light placed directly behind the cell (or sometimes at the far end) and inspect the entrance face with the beam splitter and eyepiece assembly shown in Fig. 11. The green filter is used to eliminate stray laser light. Once the beam splitter and eyepiece are fixed in place, they may be used to locate the fiber and focus on it by manipulating the cell position. This procedure is accurate to better than 25 μm; I adjust the focus further by scanning across the index dip or other sharp feature and examining the profile for sharpness. The white-light source at the far end of the fiber may be replaced with a detector for transmitted near-field scanning.

The prototype system used an ordinary three-axis translator to hold the cell. I scanned horizontally by hand and attached the micrometer to a potentiometer by means of an O

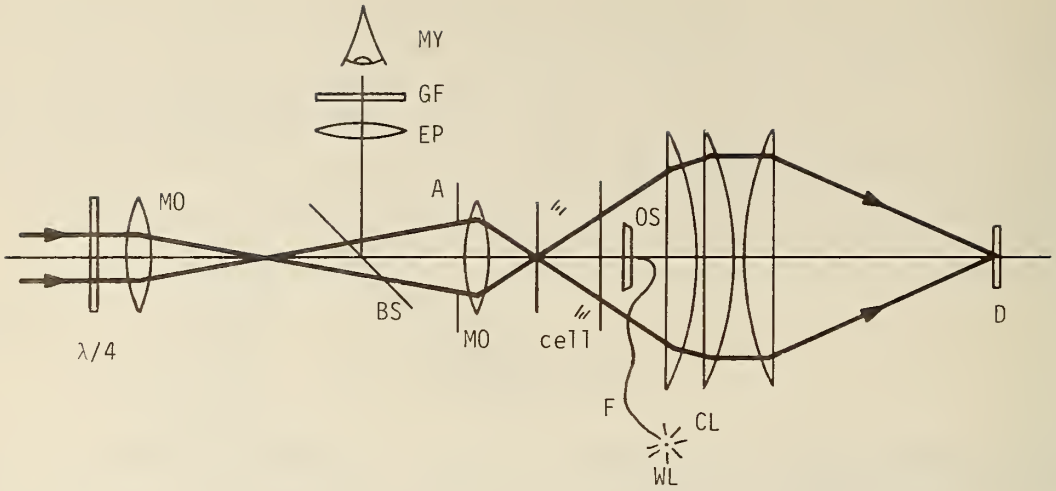

Figure 11. Experimental setup. Q--quarter-wave plate. MO--microscope objective. BS--beam splitter. A--aperture stop. OS--opaque stop. F--fiber. WL--white-light source. CL--condensing lens. D--detector. EP--eyepiece. GF--green filter. MY--experimenter.

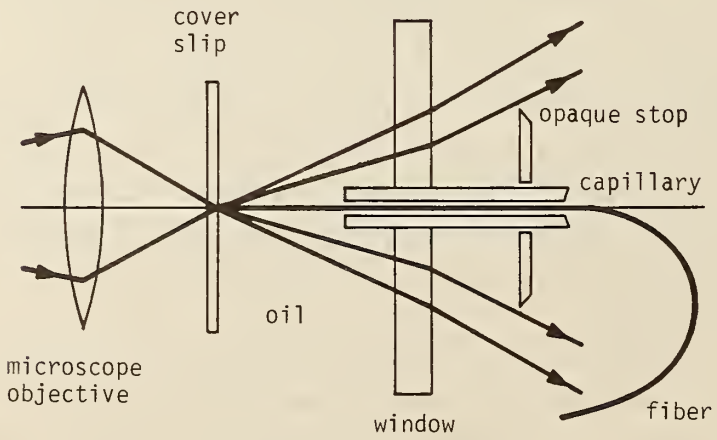

Figure 12. Detail of cell assembly and focusing optics. Outside the capillary, the fiber is confined to the plane perpendicular to the direction of scan.

Figure 13. Photograph of condensing lens.

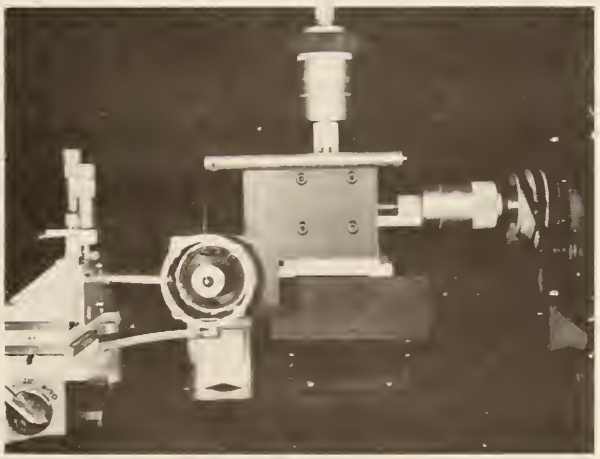

Figure 14a.

Figure 14b.

Figure 14. Photographs of the cell and translation stage, condensing lens removed.

Figure 15. Photographs of the opaque stop.

ring used as a drive belt; the potentiometer is used in a voltage-divider circuit with two batteries or a plus-and-minus 15-V power supply and drives the horizontal axis of the recorder. This system is easy to set up and may be adequate for many purposes. Because the resolution of the micrometers is 25 μm (0.001 in), the fiber may be positioned to a precision of about 6 μm; reproducibility is somewhat poorer than this figure.

I improved the prototype system by employing a 1-rpm ac motor to drive the horizontal scan of the three-axis manipulator. With a toothed wheel and matching drive belts, this system was sufficiently precise to measure the edge-response curves discussed above. For this purpose, I replaced the wire-wound 10-turn potentiometer with a continuous 1-turn potentiometer.

The system I currently employ uses a three-axis manipulator whose precision is 2.5 μm (0.0001 in) or better. I adjust the vertical and focusing axes by hand and drive the horizontal scan with the clock motor and toothed drive belts. In addition, I have made provision to scan with a translation stage driven by a digital stepping motor with 0.2 μm steps. Such a digital drive may be useful for computer analysis, but the resolution limit of 0.2 μm is insufficiently fine for much of the work reported here.

With one exception, the optical alignment of the apparatus is not critical. I introduce the laser beam by means of two mirrors (not shown). After rough alignment, I center the opaque stop by eye; the aperture stop creates pronounced diffraction rings that make the visual alignment fairly precise. After introducing the condensing lens and positioning the detector by maximizing its output, I use the mirrors to maximize the power through the system; this ensures that the laser beam is centered about the aperture stop that precedes the microscope objective. The opaque stop may be adjusted further at this time, but such adjustment does not seem necessary.

The location of the aperture stop, however, is critical. The aperture stop determines the axis of the cone that focuses onto the face of the fiber. If that axis is not very nearly parallel to the axis of the fiber, then the scans will be skewed slightly. In a graded-index fiber, the cladding index shows a slight upward or downward slope that is consistently in the same direction on both sides of the core. To correct for this error, I

found that the aperture stop must be positioned horizontally to an accuracy of 25 μm or so. With a 40X microscope objective (4-mm focal length), this corresponds to a pointing accuracy of about 6 mrad or one third of a degree. The adjustment is best made by scanning a fiber repeatedly until the cladding or the oil levels on either side of the scan are equalized. In addition, to avoid creating an angular error in the horizontal plane, I introduce the fiber by holding it in place directly above the capillary, rather than to one side.

11. CALIBRATION

Data are taken on an xy recorder. The output of the photodetector passes through a trans-impedance amplifier (current-to-voltage converter) whose output enters the vertical amplifier of the recorder. I checked the overall linearity of the electronic system by first calibrating a set of neutral-density filters at 633 nm on a spectrophotometer. Introducing the filters into the beam ahead of the first MO yielded the curve shown in Fig. 16. Electrical linearity is therefore good over a factor of at least 5.

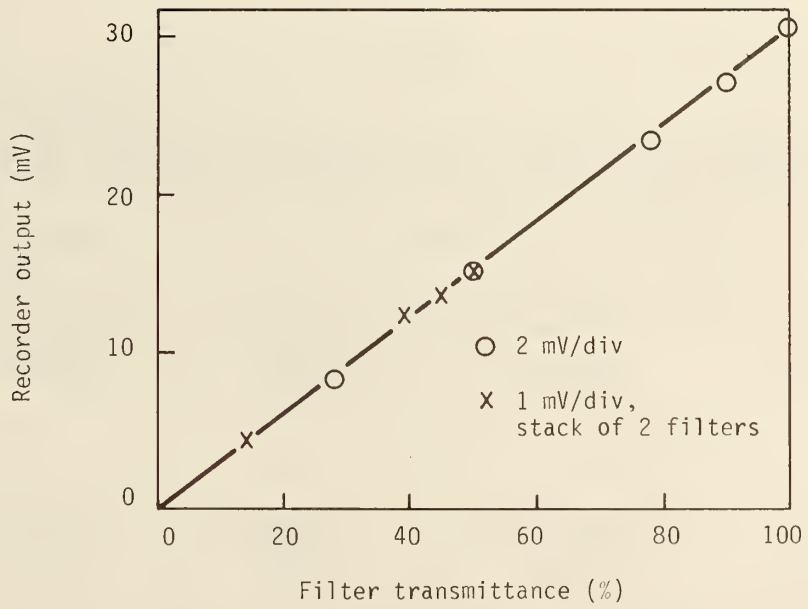

Figure 16. Electrical linearity of the system, determined by placing calibrated filters into the laser beam.

White [2] has calibrated his system by translating the stop to different positions along the axis. I sought a more-direct calibration scheme, which might be more amenable to analysis [3]. Ideally, one or more fibers with known core and cladding indices would make calibration an easy matter. Unfortunately, such a set of fibers is not available; neither

is there a guarantee that the index of a fiber is precisely that of the preform from which the fiber was drawn.

Malitson has shown that vitreous silica is manufactured with sufficient purity that the index variation from sample to sample or manufacturer to manufacturer is, for our present purposes, negligible [51]. He has also derived Sellmeier coefficients that allow calculation of the index at any wavelength up to 3.71 μm. However, Fleming has criticized the use of Malitson's numbers for calculating the index of a fiber; fibers are not annealed, but rather are chilled or quenched and may not have the same index as the annealed, bulk material [52,53]. Hence, Fleming has determined the Sellmeier coefficients relevant to quenched silica.

At the wavelength 632.8 nm, the Malitson formula gives the result that the index of the silica at 20°C is 1.457018; the Fleming formula gives 1.457334 at 23.5°C (see Table 2). Malitson quotes a temperature coefficient of $10.0 \times 10^{-6}\ K^{-1}$; thus at 23.5°C, the index of vitreous silica is 1.457053. At this temperature, the Malitson and Fleming values differ by 0.00028, an amount that is significant when compared with the accuracy to which the indices of the immersion fluids are known. I chose the average value of 1.45719 (not 1.45726 as incorrectly reported in Refs. 3 and 4) and assigned an error of ±0.00014.

Table 2

Sellmeier coefficients for vitreous silica (0.21-3.71 μm and 20°C) [49] and for quenched silica (0.44-1.53 μm and 23.5°C) [50]. All wavelengths are expressed in micrometers.

	A_1	A_2	A_3
fused silica	0.6961663	0.4079426	0.8974794
quenched silica	0.696750	0.408218	0.890815
	λ_1	λ_2	λ_3
fused silica	0.0684043	0.1162414	9.896161
quenched silica	0.069066	0.115662	9.900559

$$n^2 - 1 = \frac{A_1\lambda^2}{\lambda^2-\lambda_1^2} + \frac{A_2\lambda^2}{\lambda^2-\lambda_2^2} + \frac{A_3\lambda^2}{\lambda^2-\lambda_3^2} .$$

For calibration, I used several fibers drawn by hand from vitreous-silica rods as well as the naked core of a plastic-clad silica fiber. (Although the latter was more convenient, I wanted to verify that it was truly silica.) I compared these fibers with each of five

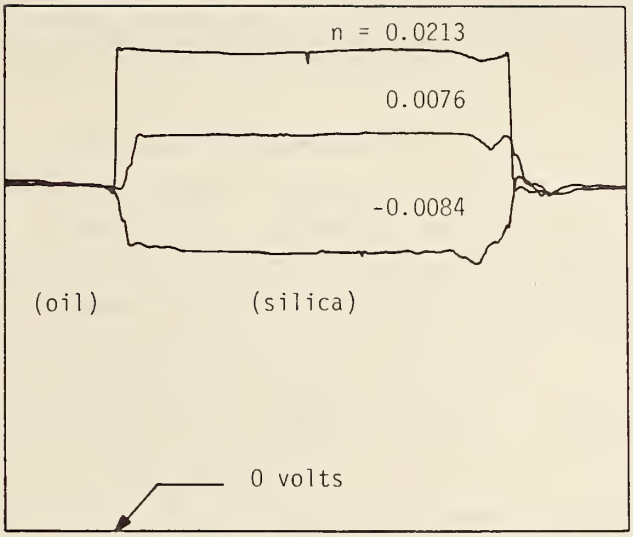

Figure 17. Calibration scans with unclad PCS fiber. Structure near right edge is a result of the fracture and does not represent true index data.

oils sequentially. The indices of the oils were supplied by the manufacturer, who claimed an accuracy of ±0.0005 [54].

Figure 17 shows a typical calibration run with the silica core. When the laser is focused into the oil rather than the fiber, the rays should emerge parallel to their original direction; we might expect the power transmitted to be independent of the index of the fluid. The slight variation in Fig. 17 may be accounted for by the change in reflectance at various oil-glass interfaces. Because of this variation, it is necessary to normalize the results to the power transmitted through the oil alone.

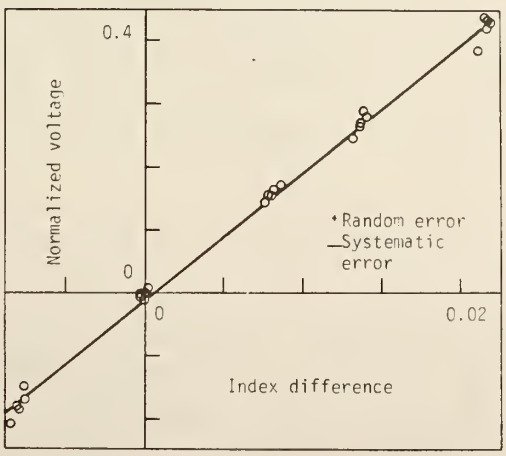

Figure 18. Normalized voltage as a function of index difference between silica and oil, for a particular stop position. Estimates of random and systematic error are indicated.

Figure 18 shows the results of some calibration runs similar to those reported in Ref. 3. The vertical axis is $(V_s - V_o)/V_o$, where V is the voltage read by the xy recorder and s and o stand for silica and oil. The horizontal axis is $n_o - n_s$, where n is index of refraction.

The greatest barrier to a linear calibration may be ensuring the absence of vignetting when the highest-index oil is in the cell (and the emergent cone was largest). It is important to verify the linearity of the system over a large range of indices in case, for example, some of the fibers to be tested have cladding indices less than that of vitreous silica. Because of the possibility of vignetting, or other effect, an extrapolation may be dangerous if linearity over a sufficient range has not been demonstrated.

A calculation along the lines described by Natrella showed linearity at the 99 percent confidence level [55]. However, I did not calculate a conventional line of best fit because the points have uncertainty in the horizontal direction as well as the vertical. Rather, I used a method similar to another suggested by Natrella. The center of mass of all the points as well as the means of each of the four sets are calculated. Three line segments join adjacent means, and their slopes are calculated. The best-fit line is taken to be the one that passes through the center of mass and whose slope is equal to the average of the slopes of the three line segments. This is the line shown in Fig. 18.

The vertical error bar in Fig. 18 is an estimate of the instrumental limit of error (or resolution) of the xy recorder; the actual vertical errors are also of this order. The horizontal error is the sum of the index uncertainties just mentioned, as well as an additional ± 0.0001 owing to the effect on the oils of the uncertainty of the oil temperature measurement. Because the large horizontal error bar is not reflected in large vertical scatter, I conclude that most if not all of the horizontal error (except the temperature component) is a systematic error that is common to each oil and has approximately constant magnitude and sign; the two horizontal error bars show the random and systematic errors separately. (See Table 3 for a compilation.)

When running an unknown sample, I usually choose the oil whose index at 25°C is about 1.464; generally this value is slightly higher than the cladding index, and the values of $\Delta V/V$ for the scan remain within the range defined by Fig. 18. In the unusual event that some of the values fell outside that range, the oil would have to be changed to avoid having to extrapolate the line in Fig. 18.

After running the scan, I remove the fiber to determine the voltage corresponding to the index of the oil without the complicating effect of the shadow of the fiber. (It is equivalent to continue to scan for several fiber radii beyond the cladding.) I measure the voltage difference corresponding to the core-cladding index difference and compute $\Delta V/V$ for the fiber. The value can be converted directly to index difference by using the slope of the calibration curve of Fig. 18. For relative measurements, it is not necessary to know the precise index of the oil; therefore, Δn should be accurate to ±0.0006, as detailed in Table 3. Because it eliminates the index of the oil from the measurement, this procedure is more accurate than calibrating each measurement with a vitreous silica fiber and monitoring the temperature of the oil.

The approximate index of the fiber is needed to calculate the numerical aperture, $NA = \sqrt{(2n^2\Delta n)}$. However, because n is large, an error in n is not nearly so severe as an error in Δn, and the NA may be calculated precisely with only approximate knowledge of the index of the fluid.

Table 3

Error Budget

Vertical		
Instrumental limit of error	±0.01	random
Horizontal		
Temperature coefficient of refractive index, ±0.25 K	±0.0001	random
Index of silica	±0.00014	systematic
Index of oils at 25°C	±0.0005	assumed systematic
SUBTOTALS	±0.0001	random
	±0.00064	systematic
Projection of vertical error	±0.0005	random
TOTALS	±0.0006	random
	±0.0006	systematic

The index of any of the oils is significantly temperature dependent; for the D line, the coefficient is of the order of $4 \times 10^{-4}\ K^{-1}$. Thus, with slight increase in complexity, we could calibrate the system using only a single oil and varying its temperature by a few tens of kelvins while measuring to a precision of a few tenths of a kelvin.

With this scheme, we could get many more points along the calibration curve, but would have to measure the index of the oil as a function of temperature at precisely the wavelength of interest. Further thoughts on index measurements of liquids are detailed in Appendices A and B.

12. MEASUREMENTS ON ACTUAL FIBERS

In this section, I report the results of refracted-ray scans of a number of actual communication fibers, on a comparison with conventional near-field scans, and on a comparison with another laboratory.

I obtained a step fiber, designated DF-1, that had been subjected to an exit-face scan and a far-field scan by other workers in this laboratory [56]. I performed additionally a refracted-ray scan and an entrance-face scan on this fiber.

Figure 19a shows the refracted-ray scan. The scan reveals a central structure that is actually an index dip surrounded by a nearly circular index dip (as may be verified with the eyepiece). In addition, the scan shows that the fiber has a low-index cladding layer surrounded by what is evidently silica.

Incidentally, if we knew that the outermost layer of a fiber were in reality silica, then we could use the index of that layer as a calibration level. Most of the fibers I have tested had cladding indices that were (within experimental accuracy) equal to that of silica; some, however, had substantially lower index. It is therefore unwise to presume anything about the fiber in the absence of a priori knowledge that it is clad with pure silica.

The apparently high-index region near the edge of the core of the fiber DF-1 is an artifact that results from the presence of leaky rays. That the structure is not real may be verified by translating the opaque stop either in or out and noticing that the magnitude of the peaks varies with stop position (not shown in a figure). These artifacts may be eliminated by translating the stop axially to the proper position, but at the expense of having to recalibrate the system and probably losing resolution.

We may also use the data to calculate the core-cladding index difference Δn and employ Eq. (36) to determine the portion of the core that is free of leaky rays; this region in indicated in Fig. 19a and corresponds well with the appearance of the artifacts.

Figure 19b shows exit-face scans of both a short length and a kilometer length of this fiber, both performed at 857 nm. The upper scan nearly resolves the index dip but suffers from the leaky-ray problem. The lower scan, on the other hand, is free of leaky rays and suggests that the fiber core does indeed have a nearly constant index of refraction. However, the index dip has been greatly exaggerated (compared with Fig. 19a), probably because of mode coupling by scattering or diffraction out of the core center as a result of the long propagation distance.

Figure 19c shows entrance-face scans of short and long pieces of this fiber. To make these scans, I simply removed the condensing lens from the system and placed the output end of the fiber into an oil-filled capillary tube and brought it nearly into contact with the detector. As before, the scan of the short length shows the index dip with what is evidently its proper magnitude but suffers from the leaky-ray problem near the core edge. The scan of the longer piece, however, distorts the index dip substantially, not only by exaggerating its magnitude, but also by injecting a spike into the center of the pattern. (This spike is easily explained by noticing that, because of the oscillatory nature of the index dip, the center of the fiber contains a tiny annular waveguide. Apparently this waveguide

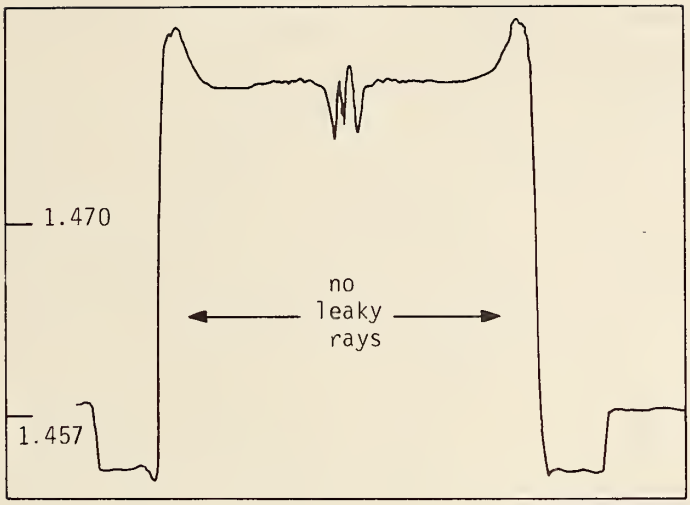

Figure 19a. Refracted-ray scan of step fiber. Arrowheads show region calculated to be free of leaky rays.

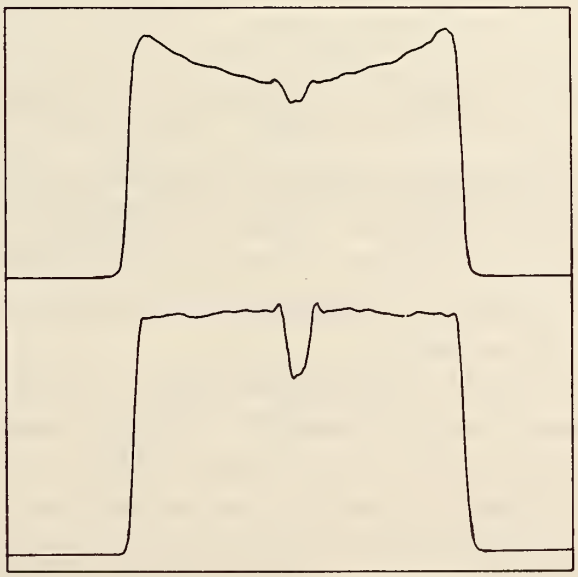

Figure 19b. Exit-face scans of step fiber at 857 nm. Upper--short length; lower--kilometer length.

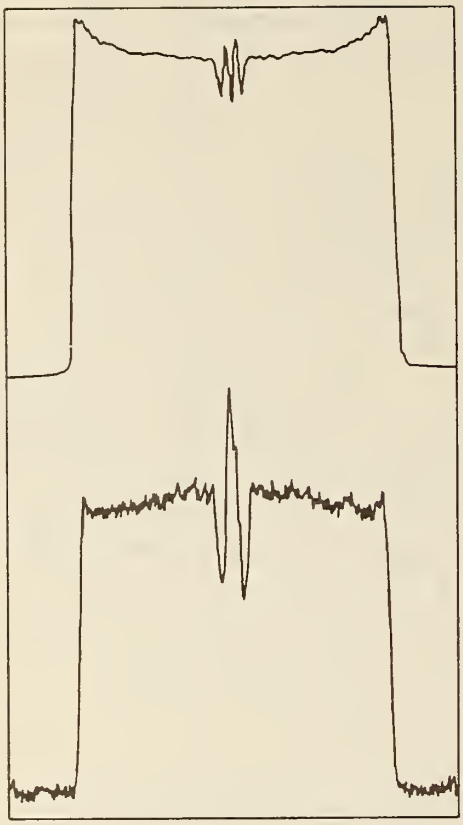

Figure 19c. Entrance-face scan of step fiber at 633 nm. Upper--short length; lower--kilometer length.

has lower loss than the fiber as a whole. The scan does not resolve the waveguide, which appears as a sharp spike.)

The refracted-ray scan shows details of the step fiber that are not shown or are distorted by conventional near-field scanning. However, the refracted-ray scan suffers from the presence of leaky rays near the periphery of the step-fiber core. It is therefore prudent, when examining step fibers, to supplement the scan with, say, entrance face scans taken with different numerical apertures.

To assess the leaky-ray problem in graded-index fibers, I performed a refracted-ray scan and an entrance-face scan of a 56-cm length of fiber DF-D; these are shown in Fig. 20. (Because the refracted-ray scan has to be inverted to make the positive n axis vertical, the upper scan is in the opposite direction from the lower two.) The horizontal scales are the same for the two scans; the vertical scales have been adjusted to give nearly the same amplitude. The cladding of fiber DF-D is not uniform, as I have determined by scanning several freshly cleaved ends; the structure in the cladding of Fig. 20 (upper) is real and not an artifact of the apparatus. Figure 20 (lower) is an exit-face scan of a long piece of the same fiber; the horizontal scale is not the same as those of Figs. 20 (upper) and (center).

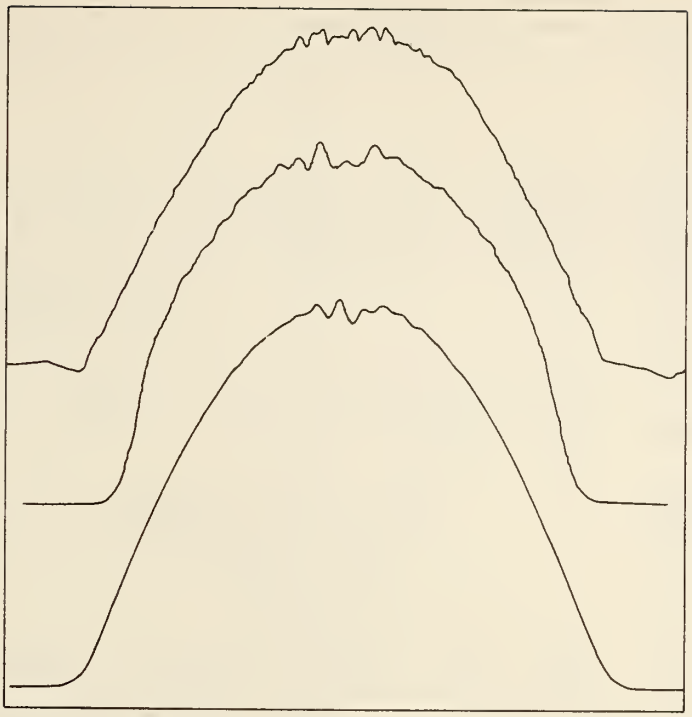

Figure 20. Scans of a graded-index fiber. Upper--refracted-ray scan; center--entrance-face scan, short length; lower--entrance-face scan, kilometer length.

Even a casual inspection shows the two near-field scans to be substantially more rounded than the refracted-ray scan.

Among the other fibers I scanned were graded-index fibers designated DF-A, B, D and E. These fibers had been used in a round robin to intercompare radiation-angle or numerical-aperture measurements made in each of several laboratories [57]. Figure 21 shows a scan of one of these fibers, DF-B. This curve is chosen deliberately to show the glitch to the left of the center, which is probably the result of a speck of dirt or a shard of glass too small to be seen with the eyepiece.

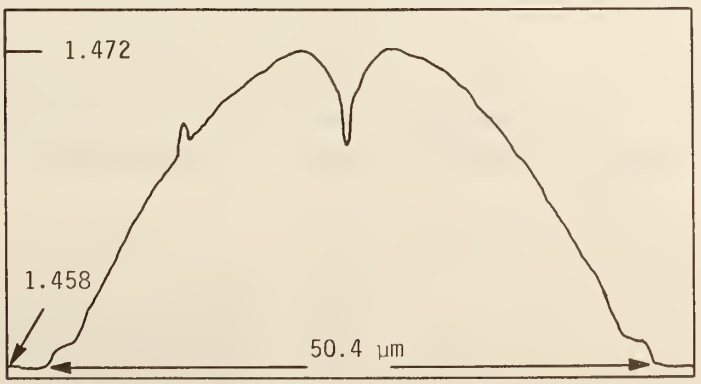

Figure 21. Refracted-ray scan of fiber DF-E. Glitch to left of center is likely due to contamination by dirt or shard of glass.

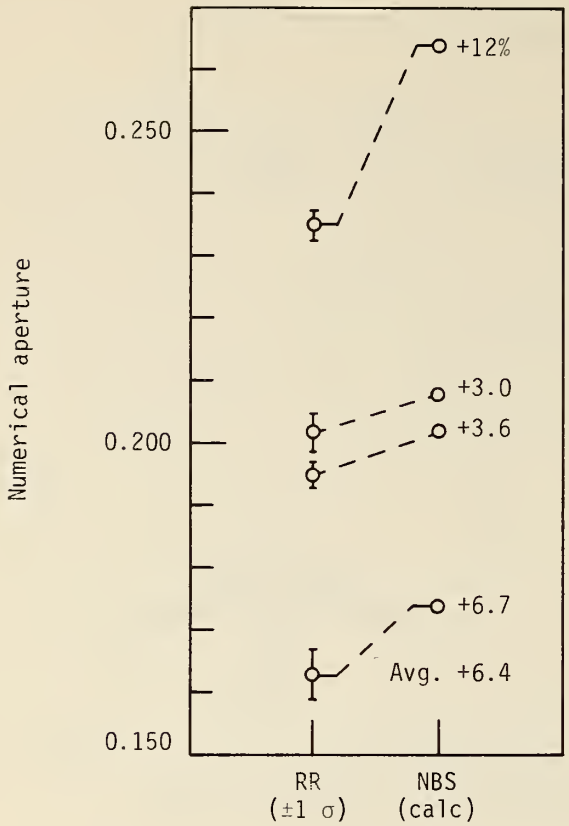

Figure 22. Comparison of numerical-aperture measurements by round robin (RR) with calculation based on index-profile measurements (NBS).

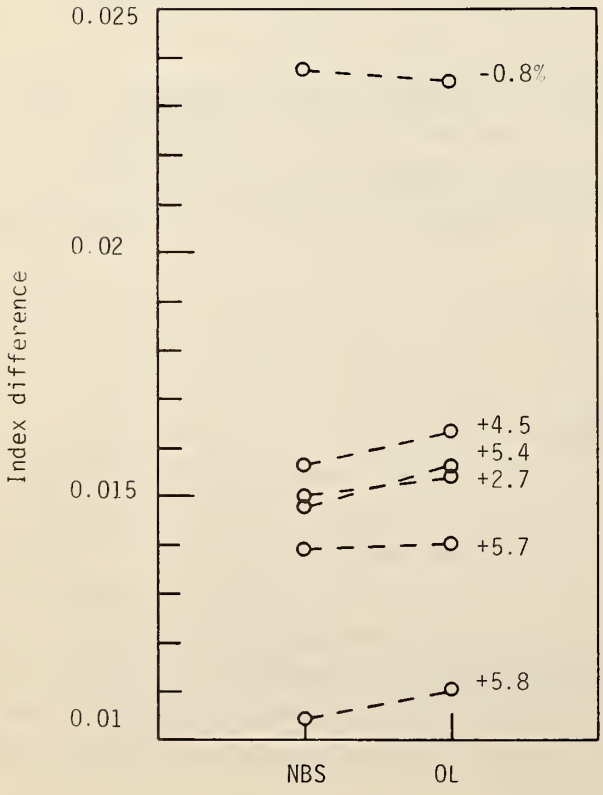

Figure 23. Core-cladding index difference measured by NBS and by other laboratory (OL) that also uses refracted-ray scanning. Average difference between measurements is 3 percent.

The maximum acceptance angle U for meridional rays is given implicitly by the formula

$$\sin^2 U = n_o^2 - n_c^2 \; ; \qquad (48)$$

sin U is sometimes called the numerical aperture of the fiber. Measured n_o and n_c and calculated sin U from Eq. (48). Table 4 compares the calculated values with the means of the values obtained for each fiber by the laboratories in the round robin. (The same data are shown graphically in Fig. 22.)

Table 4. Comparison with a Round Robin

	Numerical Aperture	
Fiber	Round-robin average [56]	Calculated, this report
DF-A	0.235 ± 2.9%*	0.264
DF-B	0.163 ± 2.4%	0.174
DF-D	0.202 ± 1.6%	0.208
DF-E	0.195 ± 0.9%	0.202

*One standard deviation, expressed in percent of mean.

In all four cases, the values calculated from index data are slightly larger than the sample-average numerical aperture. The participants in the round robin were instructed to measure the angle between the points at which the intensity was 5 percent of the peak, whereas the calculated numerical aperture will include all the light transmitted by the fiber. Therefore, we expect the calculated values to exceed slightly the measured values, and this is precisely the case.

Finally, I was fortunate to be able to make an informal comparison with M. J. Saunders of Bell Laboratories, who also uses refracted-ray scanning [58]. Owing to the round robin, which was going on at the same time, we were easily able to exchange a total of six fibers. We measured the index differences shown in Table 5 and Fig. 23. The other laboratory's value is generally slightly higher than that of NBS, but the arithmetic-average difference between our measurements is 3 percent even though we used different calibration techniques.

Table 5. Interlaboratory comparison of index difference Δn.

Fiber	This report	Other laboratory	Difference
DF-A	0.0237	0.235	-0.8%
DF-B	0.0104	0.0110	+5.8
DF-D	0.0148	0.0156	5.4
DF-E	0.0139	0.0140	0.7
MJ-A	0.0150	0.0154	2.7
MJ-B	0.0156	0.0163	4.5
		Average	+3%

13. ADDITIONAL REMARKS

One of the major practical problems with refracted-ray scanning is the accumulation of dirt particles or shards of glass on the inside of the microscope cover slip. Probably these particles are deposited by the fiber onto the inside of the capillary; they are later picked up by other fibers and deposited in turn onto the cover slip. In any case, such particles accumulate on the cover slip and eventually interfere with the measurement.

The problem may be less severe in a laboratory environment, where relatively few fibers are tested than, say, in a production environment. I simply clean the fibers in acetone after cleaving them; when the cover slip becomes contaminated with particles, I wash or replace it.

K. I. White of the British Post Office informs me that they insert their fibers by using a tube within a tube, rather than a single capillary. They push the fiber through a fine tube, cleave it, and place the tube and the fiber in an ultrasonic cleaner (which contains the same oil as the cell). They then withdraw the fiber into the tube and insert the tube into a larger tube that is fixed to the cell. They feel that much of the contamination problem is eliminated in this way.

White further informed me that their cell is cylindrical and mounted in a V block for easy removal and accurate replacement. Such a design will greatly simplify the removal and cleaning of the cover slip.

Another problem is that the fiber drifts slightly within the cell. The rate of drift varies, but is often as large as a micrometer or so per minute. With multimode fibers, this is not important unless we are interested in examining the index dip or other fine features; however, a micrometer of drift may cause significant error in a scan of a single-mode fiber.

The drift can be arrested by clamping the fiber just outside the cone of refracted rays; I simply use an alligator clip, suitably padded with a soft rubber gasket (not shown in the figures). Because the total motion of the capillary is only 100 μm or so, the alligator clip need not be fixed to the translation stage. With the fiber thus clamped, drift is very slight, whereas without clamping, the fiber sometimes drifts unacceptably before a full scan can be completed.

ACKNOWLEDGMENTS

Although I am the sole author of this Technical Note, it has been in certain ways a cooperative venture, and it is my very great pleasure to acknowledge. Eric G. Johnson for calculating the edge response of a diffraction-limited annular aperture; Ernest Kim for supplying the exit-face scans; M. J. Saunders of Bell Laboratories, Norcross, Georgia, for supplying the excellent data and the fibers with which to compare our results; Saunders, K. I. White, R. L. Gallawa, and G. W. Day for very careful and perceptive reviews; D. L. Franzen for supplying the round-robin fibers; Edie DeWeese for her infinite patience preparing the manuscript; and Aaron A. Sanders for providing means, motive, and opportunity.

APPENDIX A. MEASUREMENT OF INDEX OF REFRACTION

It may be desirable to measure the index of the matching fluids directly, for example if the calibration is to be carried out by varying the temperature of a single fluid. If a refractometer is not available, the measurement may be carried out using one of several methods that employ a prism spectrometer. The theory and practice of these methods are described in detail by Longhurst [59]. In this appendix, I will discuss several factors that limit the precision of liquid-prism and total-internal-reflection methods of measuring the index of a liquid. I include this material here because I have been unable to find similar calculations elsewhere.

There is no need to repeat Longhurst's description of the minimum-deviation method. The index is determined from the formula,

$$n = \frac{\sin\,(\alpha + \theta)/2}{\sin\,\alpha/2}\,, \tag{A1}$$

where α is the prism angle and θ is the angle of minimum deviation. At minimum deviation, $\alpha + \theta = 2I_1$, where I_1 is the angle of incidence at the first prism face, and a ray travels through the prism perpendicular to the bisector of angle α. To analyze the errors inherent in this method, we first differentiate with respect to both α and θ. The results are

$$\Delta n_\alpha = (n/2)[\cot\,\alpha/2 - \cot\,(\alpha+\theta/2]\Delta\alpha \tag{A2}$$

and

$$\Delta n_\theta = (n/2)[\cot\,(\alpha+\theta)/2]\Delta\theta, \tag{A3}$$

where Δn_α is the error that results in n if α is known to an accuracy of $\Delta\alpha$ and where Δn_θ is defined similarly. $\Delta\alpha$ and $\Delta\theta$ are instrumental errors and may be taken as one half the finest divisions on the divided circles of the spectrometer (see also Ref. 60).

For mathematical convenience, we may treat these errors as correlated and add their magnitudes to estimate the total instrumental error. Paying careful attention to sign, we find that Eqs. (A2) and (A3) are positive as written; therefore, the sum Δn_1 of the instrumental errors Δn_α and Δn_θ is

$$\Delta n_1 = (n/2)\ \Delta\alpha\ \cot\,(\alpha/2), \tag{A4}$$

where we assume that $\Delta\theta$ and $\Delta\alpha$ are equal. (Near minimum deviation, θ is a slowly varying function of angle of incidence. The orientation of the prism need be accurate no better than several minutes to measure θ precisely.)

For a 1-minute spectrometer, $\Delta\alpha = 0.5'$ or about 0.15 mrad; if $\alpha = 60°$ and $n = 1.5$, Δn_1 is consequently about 0.0002. This is about the precision required for index-profile measurements.

Taken by itself, Eq. (A4) suggests that α should be made as large as possible, provided that it is not so large that light will not pass through the prism. Figure A1, however, shows that as α increases, the deviation becomes a stronger function of angle of incidence. As a result, measurement of the minimum deviation θ becomes more dependent on the precise orientation of the prism. Inasmuch as increasing α from 60° to 80° can be expected to reduce experimental error by only about 30 percent, little or nothing will be gained by making α much larger than the common value of 60°.

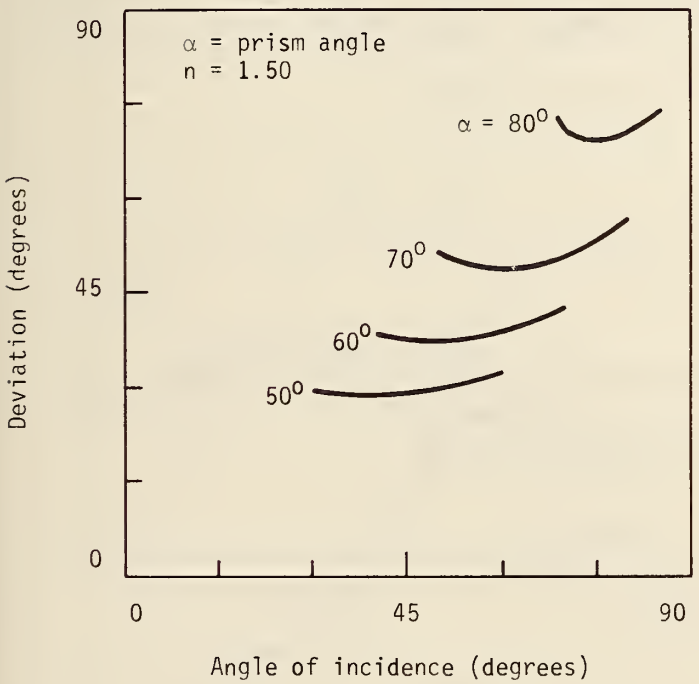

Figure A1. Deviation as a function of angle of incidence for various prism angles.

The prism must also be levelled; that is, the edge of the prism must be made parallel to the axis of rotation of the prism table. For the degree of accuracy required here, levelling error is potentially significant, as may be shown by referring to Fig. A2. In that figure, the yz plane is the plane that contains the face of the prism. The incident ray OB strikes the prism with angle of incidence i = AOB. However, because OB is inclined to the xy plane with angle ε = COB, the spectrometer will measure angle i' = AOC. We wish to calculate the difference between the measured value i' and the true value i.

We construct a vector OB whose magnitude is 1 and apply the law of cosines to the triangle OAB:

$$x^2 + 1 - 2x \cos i = x^2 + y^2 \ . \qquad \text{(A5)}$$

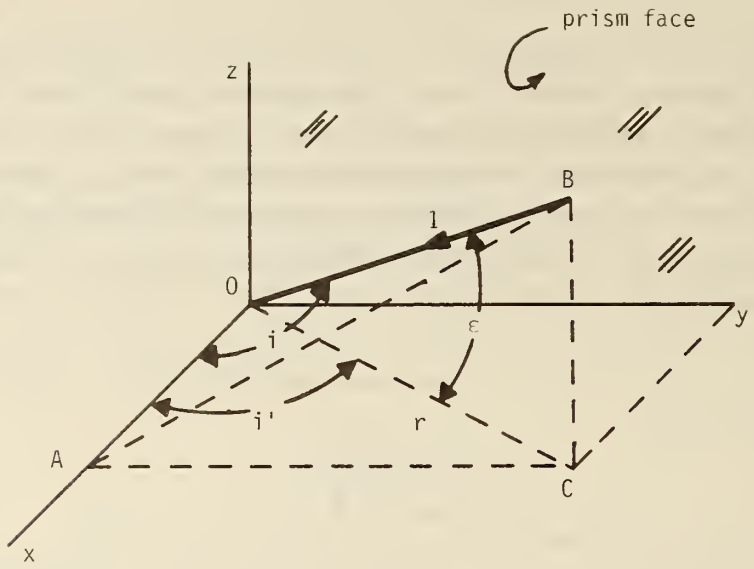

Figure A2. Geometry for calculation of error resulting from improper leveling of prism.

x, y, and z are the line segments indicated on the figure and $y^2 + z^2$ is the length of AB. We express x and y in terms of the angles ε and i', and then demand that ε be sufficiently small that $\cos \varepsilon = 1$ and $\sin \varepsilon = \varepsilon$. Eq. (A5) therefore becomes

$$\cos^2 i' + 1 - 2 \cos i' \cos i = \sin^2 i' + \varepsilon^2 . \qquad (A6)$$

When $\varepsilon = 0$, Eq. (A6) may be written in the form,

$$\cos^2 i + 1 - 2 \cos i \cos i = \sin^2 i . \qquad (A7)$$

We may combine Eqs. (A6) and (A7) by subtracting and writing the result in the form,

$$\Delta(\cos^2 i) - 2 \cos i \, \Delta(\cos i) = \Delta(\sin^2 i) + \varepsilon^2 \qquad (A8)$$

Carrying out the differentiation indicated by the symbol Δ, we find that

$$\Delta i = -\varepsilon^2/(2 \sin i \cos i). \qquad (A9)$$

At minimum deviation, α, i, and θ are related by the equation

$$\theta + \alpha = 2i. \qquad (A10)$$

The error in measuring θ is consequently twice Δi. Likewise, Fig. A2 shows that a levelling error will cause a similar error in measuring α.

Suppose that the prism has index 1.5 and that the prism angle is 60°. If we take ε to be 0.1°, then we find from Eq. (A9) that Δi is about 0.1' and therefore that $\Delta\alpha$ and $\Delta\theta$ are each about 0.2'. This is nearly comparable to the precision of the instrument used in the previous examples. Levelling must consequently be precise to better than 0.1°.

Levelling error is a systematic error and is always negative because Δi is always negative. It results in an underestimate of both θ and α, and therefore in an underestimate of n.

The index of a liquid may be measured using a hollow glass prism. The measurement will be accurate if the windows of the prism have parallel faces; in Appendix B, I show that this requirement is not stringent. Therefore, all the foregoing remarks refer to liquid-prism techniques as well as to more-common solid-prism techniques.

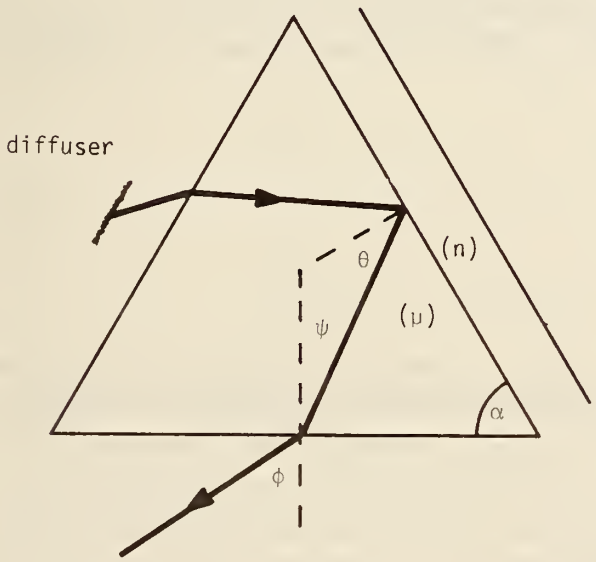

Figure A3. Critical-angle method of determining refractive index of a liquid.

It is also possible to measure the index of a liquid using a prism spectrometer and a critical-angle method, such as the two described in Ref. 54. Both methods are in principle the same; the geometry is illustrated in Fig. A3. The liquid to be measured is in contact with one face of a glass prism whose index is known. The index of the liquid is n and that of the glass is μ. μ must be greater than n if total reflection is to occur; this is not generally a serious constraint where fiber optics is concerned, because the liquids used will generally have indices less than 1.5.

The index of the liquid is found from the equation,

$$n = N \sin \alpha - \sin \phi \cos \alpha \qquad \text{(A11)}$$

derived in Ref. 54. θ is the critical angle, $N^2 = \mu^2 - \sin^2 \phi$, and other parameters are as drawn in Fig. A3.

To estimate the precision of the critical-angle methods, we differentiate Eq. (A11), yielding three equations,

$$\Delta n_\alpha = (N \cos \alpha + \sin \phi \sin \alpha)\, \Delta\alpha, \tag{A12}$$

$$\Delta n_\phi = -[(\sin \alpha \sin \phi \cos \phi)/N + \cos \alpha \cos \phi]\, \Delta\phi, \tag{A13}$$

and

$$\Delta n_\mu = (\mu/N) \sin \alpha\, \Delta\mu, \tag{A14}$$

where the notation is as before.

If we use the same example as above (namely that $\alpha = 60°$ and $\mu = 1.5$), and assume that the index of the liquid is 1.45, we find that θ is about 75° and ϕ about -23°. Therefore,

$$\Delta n_\alpha = 0.4\, \Delta\alpha,$$

$$\Delta n_\phi = -0.2\, \Delta\phi, \tag{A15}$$

and

$$\Delta n_\mu = 0.9\, \Delta\mu.$$

If $\Delta\alpha = 0.15$ mrad (0.5'), then $\Delta n_\alpha + \Delta n_\phi \sim 0.0001$. We learned in connection with Eq. (A4) that μ could be determined to 0.0002; using the critical-angle methods adds an additional uncertainty of 0.0001. If a liquid prism is available, the result may in principle be slightly more precise than a determination by the critical-angle method. However, the liquid prism I obtained commercially had such badly warped faces that I decided not to use it.

Equations (A2), (A3), (A12), (A13) and (A14) may be used for estimating the instrumental limit of error only. This represents the greatest precision that can be expected from a particular instrument. A given measurement will have to be carried out several times before the statistical limit of error is as small as the instrumental limit.

Finally, the index of typical liquids varies considerably with temperature, the coefficient being of the order of 0.0004 K^{-1}. Therefore, if the index is to be determined to greater precision than the figures assumed in this appendix, the temperature will have to be controlled to within a few tenths of a kelvin.

APPENDIX B. USE OF THE HOLLOW PRISM

A hollow prism may be used to measure the index of refraction of a liquid, provided that the glass windows have reasonably parallel faces. To determine the imprecision that results from lack of parallelism, we assume that any wedge is shared equally by the two windows through which the light passes. This is, of course, an approximation, but it allows us to draw the ray through the liquid parallel to the base of the prism when the deviation is a minimum. Only half the prism need be drawn, as in Fig. B1. In that figure, the angles are defined as indicated. The angle labeled θ is one-half the deviation brought about by the whole prism.

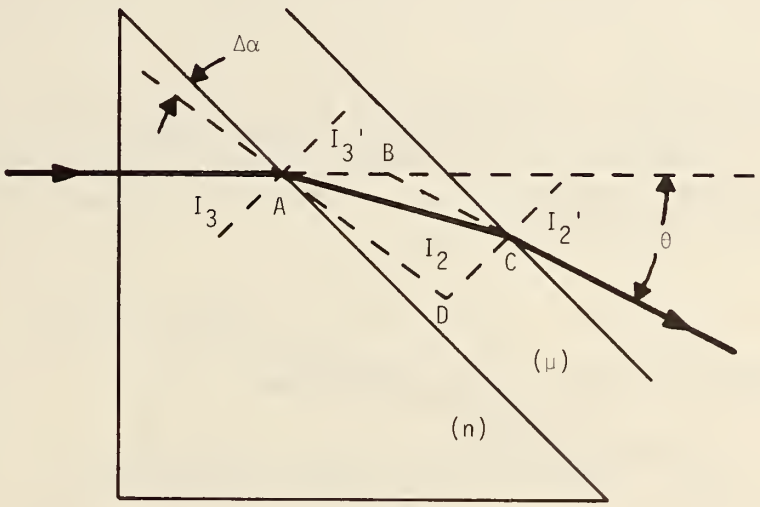

Figure B1. Geometry for calculating effect of wedge in faces of liquid prism.

If the window surfaces are parallel, then the angles are as labeled in Fig. B1. Suppose that we incline the inner face of the window by an angle $\Delta\alpha$, as shown by the dotted line. Then the angles change from I_3 to $I_3 + \Delta I_3$ and so on. We wish to calculate the change $\Delta\theta$ in θ that results from the wedge angle $\Delta\alpha$.

To begin, we apply Snell's law to the refraction at the liquid-glass interface,

$$n \sin I_3 = \mu \sin I_3' \tag{B1}$$

Differentiating both sides of Eq. (B1), we find that

$$\Delta I_3' = (n \cos I_3 / \mu \cos I_3') \, \Delta I_3 \tag{B2}$$

where ΔI_3 is equal to $\Delta\alpha$. Similarly,

$$\Delta I_2' = (\mu \cos I_2/\cos I_2')\, \Delta I_2, \tag{B3}$$

but ΔI_2 is not equal to $\Delta\alpha$.

We learn from triangle ABC that

$$\theta = I_3 - I_3' + I_2' - I_2 \tag{B4}$$

and therefore that

$$\Delta\theta = \Delta I_3 - \Delta I_3' + \Delta I_2' - \Delta I_2 \tag{B5}$$

and

$$\Delta\theta = [1 - n \cos I_3/(\mu \cos I_3')]\Delta I_3 + (\mu \cos I_2/\cos I_2' - 1)\Delta I_2. \tag{B6}$$

Using triangle ACD, we find that

$$\Delta I_2 = \Delta I_3' - \Delta\alpha, \tag{B7}$$

which we substitute into Eq. (B5). Equation (B5) becomes

$$\Delta\theta = [(n \cos I_3/\cos I_3') - \mu](\cos I_2/\cos I_2')\Delta\alpha\ . \tag{B8}$$

Even if n and μ differ by 0.1, $\cos I_3'$ is very close to $\cos I_3$, so Eq. (B8) may be simplified to

$$\Delta\theta = (n - \mu)(\cos I_2/\cos I_2')\Delta\alpha. \tag{B9}$$

If we use the same example as before, and let $n - \mu$ be 0.05, we find that

$$2\Delta\theta \sim 0.15\Delta\alpha \tag{B10}$$

where $2\Delta\theta$ is the total error of measuring the deviation and where $\Delta\alpha$ is the wedge angle of each window. Common optical windows will have wedge of 20" or so; thus, $2\Delta\theta$ is about 3" or 0.05'. Because this error is much smaller than the errors noted in Appendix A, wedge in the windows will not be a factor unless we need to know n substantially better than ±0.0002.

APPENDIX C. RESOLUTION LIMIT AND DEPTH OF FOCUS

The resolution limit of a microscope objective in air may be expressed as λ/NA, where NA is the numerical aperture and is equal to sin U; U is the angle formed by the marginal ray and the axis, as shown in Fig. C1 (see Ref. 38, Chapter 2).

As a rule (except in metallurgical microscopes), the image is projected into a medium whose index n differs from that of air. This is also shown in Fig. C1. The resolution limit RL' in the medium is equal to $\lambda'/\sin U'$, where $\lambda' = \lambda/n$ is the wavelength in the medium. Using Snell's law at the interface, we find that $\sin U = n \sin U'$. Therefore, RL' = RL. The change of U is precisely compensated by the wavelength shift. This is a well-known result, namely that the resolution limit is λ/NA, independent of the index of the surrounding material.

The depth of focus DF is given by $\lambda/2(NA)^2 = \lambda/2\sin^2 U$. (That is, the image is in acceptable focus within a distance $\pm DF$ of the image point.) The depth of focus DF' in the medium is therefore $\lambda'/2 \sin^2 U'$, which reduces to $DF' = nDF = n\lambda/2(NA)^2$. The change of wavelength does not compensate the change of angle, and depth of focus is larger in the medium by a factor of n.

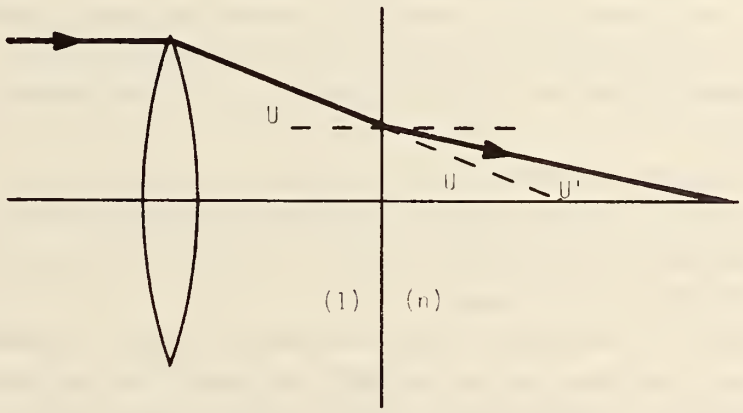

Figure C1. Geometry used for determining the resolution limit in matching fluid.

REFERENCES

[1] Stewart, W. J., A new technique for measuring the refractive index profiles of graded optical fibers, Proc. Conf. Integrated Optics and Optical Communication, Japan, 395-398 (1977).

[2] White, K. I., Practical application of the refracted near-field technique for the measurement of optical fibre refractive index profiles, Opt. and Quantum Elect. 11:185-196 (1979).

[3] Young, M., Calibration technique for refracted near-field scanning of optical fibers, Appl. Opt. 19:2479-80 (1980).

[4] Young, M., Linearity and resolution of refracted near-field scanning, Technical digest --Symposium on optical fiber measurements, 1980, NBS Spec. Pub. 597 (1980). Available from Supt. of Documents, U.S. Govt. Printing Office, Washington, DC 20402, USA.

[5] Liu, Y. S., Direct measurement of refractive indices for a small numerical aperture cladded fiber: A simple method, Appl. Opt. 13:1255-1256 (1974).

[6] Marhic, M. E., Ho, P. S., and Epstein, M., Nondestructive refractive-index profile measurements of clad optical fibers, Appl. Phys. Lett. 26:574-575 (1975).

[7] Saunders, M. J., and Gardner, W. B., Nondestructive interferometric measurement of the delta and alpha of clad optical fibers, Appl. Opt. 16:2368-2371 (1977).

[8] Stone, F. T., Rapid optical fiber delta measurement by refractive index tuning, Appl. Opt. 16:2738-2742 (1977).

[9] Hanson, A. G., Bloom, L. R., Day, G. W., Gallawa, R. L., Gray, E. M., and Young, M., Optical waveguide communications glossary, National Telecommunications and Information Administration Publication NTIA-SP-79-4 (1979). I try at all times to use the terminology set forth in this document.

[10] Maruyama, Y., Iwata, K., and Nagata, R., Determination of axially symmetric refractive index distribution from directions of emerging rays, Appl. Opt. 16:2500-2503 (1977).

[11] Iga, K., and Kokobun, Y., Formulas for calculating the refractive index profile of optical fibers from their transverse interference patterns, Appl. Opt. 17:1972-1974 (1978).

[12] Okoshi, T., and Hotate, K., Refractive-index profile of an optical fiber: Its measurement by the scattering-pattern method, Appl. Opt. 15:2756-2764 (1976).

[13] Chu, P. L., and Whitbread, T., Nondestructive determination of refractive index profile of an optical fiber: Fast Fourier transform method, Appl. Opt. 18:1117-1122 (1979).

[14] Saekeang, C., and Chu, P. L., Nondestructive determination of refractive index profile of an optical fiber: Backward light scattering method, Appl. Opt. 18:1110-1116 (1979).

[15] Marcuse, D., Refractive index determination by the focusing method, Appl. Opt. 18:9-13 (1979).

[16] Marcuse, D., and Presby, H. M., Focusing method for nondestructive measurement of optical fiber index profiles, Appl. Opt. 18:14-22 (1979).

[17] Presby, H. M., Marcuse, D., and French, W. G., Refractive-index profiling of single-mode optical fibers and preforms, Appl. Opt. 18:4006-4011 (1979).

[18] Presby, H. M., and Kaminow, I. P., Binary silica optical fibers: Refractive index and profile dispersion measurements, Appl. Opt. 15:3029-3036 (1976).

[19] Martin, W. E., Refractive index profile measurement of diffused optical waveguides, Appl. Opt. 13:2112-2116 (1974).

[20] Wonsiewicz, B., French, W., Lazay, P., and Simpson, J., Automatic analysis of interferograms: optical waveguide refractive index profiles, Appl. Opt. 15:1048 (1976).

[21] Eickhoff, W., and Weidel, E., Measuring method for the refractive index profile of optical glass fibers, Opt. and Quantum Elect. 7:109-113 (1975).

[22] Calzavara, M., Costa, B., and Sordo, B., Stability and noise improvement in reflectometric index measurement, Post-deadline paper, Symposium on Optical Fiber Measurements, 1980, NBS Spec. Pub. 597 (1980).

[23] Tateda, M., Single-mode-fiber refractive-index profile measurement by reflection method, Appl. Opt. 17:475-478 (1978).

[24] Maeda, K., and Hamasaki, J., A method of determining the refractive index profile of a lenslike medium, J. Opt. Soc. Amer. 67:1672-1680 (1977).

[25] Brinkmeyer, E., Refractive-index profile determination of optical fibers from the diffraction pattern, Appl. Opt. 16:2802-2803 (1977); Refractive index profile determination of optical fibers by spatial filtering, Appl. Opt. 17:14-15 (1978).

[26] Jeunhomme, L., and Pocholle, P., Selective mode excitation of graded index optical fibers, Appl. Opt. 17:463-468 (1978).

[27] Rawson, E. G., and Murray, R. G., Interferometric measurement of SELFOC dielectric constant coefficients to sixth order, IEEE J. Quant. Elect. QE9:1114-1118 (1973).

[28] Daino, B., Piazzola, S., and Sagnotti, A., Spatial coherence and index-profiling in optical fibers, Opt. Act. 26:923-928 (1979).

[29] Marcuse, D. and Presby, H. M., Index profile measurements of fibers and their evaluation, Proc. IEEE 68:666-688 (1980).

[30] Gloge, D., and Marcatili, E. A. J., Multimode theory of graded-core fibers, Bell Syst. Tech. J. 52:1563-1578 (1973).

[31] Payne, D. N., Sladen, F. M. E., and Adams, M. J., Index profile determination in graded index fibres, Proc. First Conf. on Optical Fibre Communication, London, IEE Pub. 132, 43-45 (1975).

[32] Payne, D. N., Sladen, F. M. E., and Adams, M. J., Determination of optical fiber refractive index profiles by a near-field scanning technique, Appl. Phys. Lett. 28:255-258 (1976).

[33] Adams, M. J., Payne, D. N. and Sladen, F. M. E., Correction factors for the determination of optical-fibre refractive-index profiles by the near-field scan technique, Electron, Lett. 12:281-283 (1976).

[34] Adams, M. J., Payne, D. N., and Sladen, F. M. E., Length-dependent effects due to leaky modes on multimode graded-index optical fibers, Opt. Commun. 17:204-209 (1976).

[35] Arnaud, J. A., and deRosier, R. M., Novel technique for measuring the index profile of optical fibers, Bell Syst. Tech. J. 55:1489-1508 (1976).

[36] Sumner, G. T., A new technique for refractive index profile measurement in multimode optical fibres, Opt. and Quantum Elect. 9:79-82 (1977).

[37] Petermann, K., Uncertainties of the leaky mode correction for near-square-law optical fibers, Electron. Lett. 13:513-514 (1977).

[38] Young, M., Optics and lasers, an engineering physics approach, Springer, New York, Berlin, Heidelberg (1977) Chap. 3.

[39] Snyder, A. W., Leaky-ray theory of optical waveguides of circular cross section, Appl. Phys. 4:273-298 (1974).

[40] Snyder, A. W., Mitchell, D. J., and Pask, C., Failure of geometric optics for analysis of circular fibers, J. Opt. Soc. Am. 64:608-614 (1974).

[41] Snyder, A. W., and Mitchell, D. J., Leaky rays on circular optical fibers, J. Opt. Soc. Amer. 64:615-623 (1974).

[42] Born, M., and Wolf, E., Principles of optics, 2nd revised ed., MacMillan, New York (1964), pp. 416-417.

[43] Gaskill, J. D., Linear systems, Fourier transforms, and optics, Wiley, New York (1978), pp. 343-345.

[44] I am greatly indebted to my friend, Eric G. Johnson, for carrying out numerical integrations of equations (37) and (38).

[45] Kermisch, D., Principle of equivalence between scanning and conventional optical imaging systems, J. Opt. Soc. Amer. 67:1357-1360; 1977.

[46] Young, M., Ref. 35, pp. 125-128. Martin, L. C., Technical Optics, Vol. 2, 2nd edition, Sir Isaac Pitman and Sons, Ltd., London (1960), pp. 146-147.

[47] Martin, L. C., Ref. 46.

[48] Stewart, W. J., Resolution of near-field optical fibre refractive index profiling methods, Proc. International Meeting on Scanned Image Microscopy, London, 1980, Academic Press, New York (1981), pp. 233-239.

[49] Reid, D. C. J. and Stewart, W. J., Ultrahigh resolution refractive near-field profiling, Proc. Conf. Integrated Optics and Optical Communications, San Francisco, CA (1981), pp. 64-66.

[50] Reference 38, p. 17.

[51] Malitson, I. H., Interspecimen comparison of the refractive index of fused silica, J. Opt. Soc. Am. 55:1205-1209 (1965).

[52] Fleming, J. W., Material dispersion in lightguide glasses, Electron. Lett. 14, 326-329 (1978).

[53] Fleming, J. W., Dispersion in step-index silicone-clad fibers, Appl. Opt. 18, 4000-4002 (1979).

[54] I am indebted to Michael Liva and William Sacher of Cargille Laboratories for providing the liquids along with their indices, their Sellmeier coefficients and a statement of accuracy.

[55] Natrella, M. G., Experimental Statistics, NBS Handbook 91, 5-22, 5-23, 5-27 (1963).

[56] Ernest Kim very kindly supplied the exit-face scans.

[57] Kim, E. and Franzen, D. L., Interlaboratory measurement comparison to determine the radiation angle (NA) of graded-index optical fibers, Appl. Opt. 20:1218-1220, 1981.

[58] Saunders, M. J., Optical fiber profiles using the refracted near-field technique: a comparison with interferometry, Technical Digest--Symposium on Optical Fiber Measurements, 1980, Digest supplement, available from Optical Electronic Metrology Group, U.S. National Bureau of Standards, Boulder, CO 80303; see also Ref. 4 for complete digest.

[59] Longhurst, R. S., Geometrical and physical optics, 3rd ed., Longmans Group, London (1973), chap. 5.

[60] Tilton, L. W. Standard conditions for precise prism refractometry, J. Res. Nat. Bur. Stds. 14:393-418; 1935. Tilton, L. W. Prism refratormetry and certain goniometrical requirements for precision, J. Res. Nat. Bur. Stds. 2:909-930; 1929.

NBS-114A (REV. 9-78)

U.S. DEPT. OF COMM. BIBLIOGRAPHIC DATA SHEET	1. PUBLICATION OR REPORT NO. NBS TN-1038	2. Gov't. Accession No.	3. Recipient's Accession No.

4. TITLE AND SUBTITLE
REFRACTED-RAY SCANNING (REFRACTED NEAR-FIELD SCANNING) FOR MEASURING INDEX PROFILES OR OPTICAL FIBERS

5. Publication Date
May 1981

6. Performing Organization Code

7. AUTHOR(S)
Matt Young

8. Performing Organ. Report No.

9. PERFORMING ORGANIZATION NAME AND ADDRESS

NATIONAL BUREAU OF STANDARDS
DEPARTMENT OF COMMERCE
WASHINGTON, D.C. 20234 Boulder, Colorado 80303

10. Project/Task/Work Unit No.

11. Contract/Grant No.

12. SPONSORING ORGANIZATION NAME AND COMPLETE ADDRESS *(Street, City, State, ZIP)*
Supported in part by the Department of Defense, Calibration Coordination Group (CCG).

13. Type of Report & Period Covered

14. Sponsoring Agency Code

15. SUPPLEMENTARY NOTES

☐ Document describes a computer program; SF-185, FIPS Software Summary, is attached.

16. ABSTRACT *(A 200-word or less factual summary of most significant information. If document includes a significant bibliography or literature survey, mention it here.)*

The purpose of this work is twofold. First, it provides an elementary description and tutorial overview of the new refracted-ray method of measuring fiber-index profiles. Second, it presents new results concerning the theoretical foundation, the linearity and precision, resolution limit and edge response, and other aspects of the method. In particular, we find that index differences may be measured to 5 percent or better and spatial resolution is diffraction limited. We conclude by showing about 3 percent agreement with another laboratory and good agreement with numerical-aperture measurements performed by participants in a round-robin experiment.

17. KEY WORDS *(six to twelve entries; alphabetical order; capitalize only the first letter of the first key word unless a proper name; separated by semicolons)*
Fiber index profile; index profile; near-field scanning; optical communications; optical fiber; optical waveguide; refracted near-field scanning; refracted-ray scanning; resolution limit.

18. AVAILABILITY ☐ Unlimited

☐ For Official Distribution. Do Not Release to NTIS

☒ Order From Sup. of Doc., U.S. Government Printing Office, Washington, DC 20402

☐ Order From National Technical Information Service (NTIS), Springfield, VA 22161

19. SECURITY CLASS (THIS REPORT)
UNCLASSIFIED

21. NO. OF PRINTED PAGES
56

20. SECURITY CLASS (THIS PAGE)
UNCLASSIFIED

22. Price
$3.75

NBS TECHNICAL PUBLICATIONS

PERIODICALS

JOURNAL OF RESEARCH—The Journal of Research of the National Bureau of Standards reports NBS research and development in those disciplines of the physical and engineering sciences in which the Bureau is active. These include physics, chemistry, engineering, mathematics, and computer sciences. Papers cover a broad range of subjects, with major emphasis on measurement methodology and the basic technology underlying standardization. Also included from time to time are survey articles on topics closely related to the Bureau's technical and scientific programs. As a special service to subscribers each issue contains complete citations to all recent Bureau publications in both NBS and non-NBS media. Issued six times a year. Annual subscription: domestic $13; foreign $16.25. Single copy, $3 domestic; $3.75 foreign.

NOTE: The Journal was formerly published in two sections: Section A "Physics and Chemistry" and Section B "Mathematical Sciences."

DIMENSIONS/NBS—This monthly magazine is published to inform scientists, engineers, business and industry leaders, teachers, students, and consumers of the latest advances in science and technology, with primary emphasis on work at NBS. The magazine highlights and reviews such issues as energy research, fire protection, building technology, metric conversion, pollution abatement, health and safety, and consumer product performance. In addition, it reports the results of Bureau programs in measurement standards and techniques, properties of matter and materials, engineering standards and services, instrumentation, and automatic data processing. Annual subscription: domestic $11; foreign $13.75.

NONPERIODICALS

Monographs—Major contributions to the technical literature on various subjects related to the Bureau's scientific and technical activities.

Handbooks—Recommended codes of engineering and industrial practice (including safety codes) developed in cooperation with interested industries, professional organizations, and regulatory bodies.

Special Publications—Include proceedings of conferences sponsored by NBS, NBS annual reports, and other special publications appropriate to this grouping such as wall charts, pocket cards, and bibliographies.

Applied Mathematics Series—Mathematical tables, manuals, and studies of special interest to physicists, engineers, chemists, biologists, mathematicians, computer programmers, and others engaged in scientific and technical work.

National Standard Reference Data Series—Provides quantitative data on the physical and chemical properties of materials, compiled from the world's literature and critically evaluated. Developed under a worldwide program coordinated by NBS under the authority of the National Standard Data Act (Public Law 90-396).

NOTE: The principal publication outlet for the foregoing data is the Journal of Physical and Chemical Reference Data (JPCRD) published quarterly for NBS by the American Chemical Society (ACS) and the American Institute of Physics (AIP). Subscriptions, reprints, and supplements available from ACS, 1155 Sixteenth St., NW, Washington, DC 20056.

Building Science Series—Disseminates technical information developed at the Bureau on building materials, components, systems, and whole structures. The series presents research results, test methods, and performance criteria related to the structural and environmental functions and the durability and safety characteristics of building elements and systems.

Technical Notes—Studies or reports which are complete in themselves but restrictive in their treatment of a subject. Analogous to monographs but not so comprehensive in scope or definitive in treatment of the subject area. Often serve as a vehicle for final reports of work performed at NBS under the sponsorship of other government agencies.

Voluntary Product Standards—Developed under procedures published by the Department of Commerce in Part 10, Title 15, of the Code of Federal Regulations. The standards establish nationally recognized requirements for products, and provide all concerned interests with a basis for common understanding of the characteristics of the products. NBS administers this program as a supplement to the activities of the private sector standardizing organizations.

Consumer Information Series—Practical information, based on NBS research and experience, covering areas of interest to the consumer. Easily understandable language and illustrations provide useful background knowledge for shopping in today's technological marketplace.

Order the **above** *NBS publications from: Superintendent of Documents, Government Printing Office, Washington, DC 20402.*

Order the **following** *NBS publications—FIPS and NBSIR's—from the National Technical Information Services, Springfield, VA 22161.*

Federal Information Processing Standards Publications (FIPS PUB)—Publications in this series collectively constitute the Federal Information Processing Standards Register. The Register serves as the official source of information in the Federal Government regarding standards issued by NBS pursuant to the Federal Property and Administrative Services Act of 1949 as amended, Public Law 89-306 (79 Stat. 1127), and as implemented by Executive Order 11717 (38 FR 12315, dated May 11, 1973) and Part 6 of Title 15 CFR (Code of Federal Regulations).

NBS Interagency Reports (NBSIR)—A special series of interim or final reports on work performed by NBS for outside sponsors (both government and non-government). In general, initial distribution is handled by the sponsor; public distribution is by the National Technical Information Services, Springfield, VA 22161, in paper copy or microfiche form.

U.S. DEPARTMENT OF COMMERCE
National Bureau of Standards
Washington, D.C. 20234

OFFICIAL BUSINESS

Penalty for Private Use, $300

POSTAGE AND FEES PAID
U.S. DEPARTMENT OF COMMERCE
COM-215

SPECIAL FOURTH-CLASS RATE
BOOK